Forest Ecology and Management 375 (2016) 279–308

Contents lists available at ScienceDirect

Forest Ecology and Management

journal homepage: www.elsevier.com/locate/foreco

Emergent crowns and light-use complementarity lead to global maximum biomass and leaf area in *Sequoia sempervirens* forests

Robert Van Pelt [a,b,*], Stephen C. Sillett [a,b], William A. Kruse [c], James A. Freund [b], Russell D. Kramer [b]

[a] Department of Forestry and Wildland Resources, Humboldt State University, Arcata, CA 95521, USA
[b] School of Environmental and Forest Sciences, College of the Environment, University of Washington, Box 352100, Seattle, WA 98195, USA
[c] Kruse Imaging, 3230 Ross Rd., Palo Alto, CA 94303, USA

ARTICLE INFO

Article history:
Received 23 January 2016
Received in revised form 9 May 2016
Accepted 13 May 2016

Keywords:
Sequoia sempervirens
Old growth
Forest structure
Biomass
LAI
Leaf area
Carbon sequestration
LiDAR
Emergent trees
Heartwood
Allometric equations
Light-use complementarity

ABSTRACT

Forests >80 m tall have the highest biomass, and individual trees in these forests are Earth's largest with deep crowns emerging above neighboring vegetation, but it is unclear to what degree these maxima depend on the emergent trees themselves or a broader-scale forest structure. Here we advance the concept of *emergent facilitation*, whereby emergent trees benefit co-occurring species. Trees reorganize foliage within crowns to optimize available light and, if long-lived, can reiterate after crown damage to become emergent. The height, depth, and spacing of emergent trees in turn allows for abundant light to pass through the canopy, leading to light-use complementarity as well as elevated biomass, leaf area, and species diversity of the forest as a whole. We chose *Sequoia sempervirens* to develop this concept and installed eleven 1-ha plots in old-growth forests spanning nearly six degrees of latitude in California. Each plot was based off a 316-m-long centerline where biomass and leaf area of all vegetation were quantified. We employed hierarchical measurements and stratified random sampling spanning the full size range of individuals to generate 180 equations for determining biomass and leaf area of all dominant plant species in these forests. Biomass (5190 Mg ha^{-1}), leaf area (LAI = 19.4), and aboveground carbon (2600 Mg ha^{-1}) are global maxima, occurring in plots with the highest proportion of emergent trees. Decay-resistant *Sequoia* heartwood contributes the bulk of this mass, ranging from 61.5 to 76.7% of plot totals. Heartwood is a key contributor to the development of trees with emergent crowns, since its durability enables trees to recover leaf area and to re-grow crowns after damage so that they can continue expanding for millennia. By distributing leaf area among fewer trees with deeper crowns, *Sequoia* maintains very high leaf area itself (LAI up to 14.5) while simultaneously allowing other species to flourish underneath (non-*Sequoia* LAI up to 8.0). Because *Sequoia* is not replaced by other species, aboveground biomass, leaf area, and carbon content of these forests are essentially asymptotic over time.

1. Introduction

Globally, the tallest forests also have the highest biomass (Waring and Franklin, 1979; Keith et al., 2009). Forests with trees >80 m tall all have abundant precipitation and most occur at low elevations, but the same holds true for many other forests that do not produce tall trees (Tng et al., 2012). Beyond elevation and precipitation, an optimal temperature regime – specifically low seasonal variation in temperature – is a global determinant of maximum tree height (Larjavaara and Muller-Landau, 2011). Wet, low elevation forests with mild and stable temperature regimes only occur in coastal environments, and accordingly nearly all trees >80 m tall grow within 100 km of an ocean with most being much closer (Larjavaara, 2013).

Biomass and leaf area of the tallest forests are often more than an order of magnitude higher than shorter forests, including those in tropical Central and South America as well as those in temperate Europe and eastern North America (Franklin and Waring, 1980; Keith et al., 2009). The largest trees consistently occur in forests with near-maximum biomass and leaf area (Sillett and Van Pelt, 2007; Sillett et al., 2015b). Linkages between large trees and forest structure are so strong that aboveground biomass in Central African forests is predictable with information from only the largest 5% of their trees (Bastin et al., 2015). Large trees are a critical element of forest structure, but it is unclear to what degree maximum biomass and leaf area are attributable to the presence of large trees or a broader-scale forest structure. Even in

* Corresponding author at: Department of Forestry and Wildland Resources, Humboldt State University, Arcata, CA 95521, USA.
E-mail address: abies2@u.washington.edu (R. Van Pelt).

http://dx.doi.org/10.1016/j.foreco.2016.05.018
0378-1127/

high-biomass forests dominated by a single species, other species often substantially contribute to plot-level leaf area (Grier and Logan, 1977; Van Pelt et al., 2004). Massive accumulation of biomass in living trees is also associated with large logs and snags that can represent as much as one-third of total forest carbon (Smithwick et al., 2002; Burrascano et al., 2013), especially in cool temperate rainforests (*sensu* Alaback, 1991) where saturated logs have slow rates of decay (Harmon et al., 1986; Daniels et al., 1997).

1.1. Crown development of tall trees

The six species in the world verified >90 m tall represent the two largest members of three families and two phyla (Table 1). Achieving these dimensions not only requires an immense leaf area, but also an optimal scaffolding on which to array leaves. Trees with the highest leaf areas are those that can maintain foliage in shade and develop deep crowns (Horn, 1971; Leverenz and Hinckley, 1990). The tallest *Cupressaceae* (*Sequoia sempervirens* and *Sequoiadendron giganteum*) are the only known trees to support leaf dry masses >900 kg (Sillett et al., 2015a), and among 30 crown-mapped trees with this much foliage, mean crown depths are >60 m with crown-depth-to-diameter ratios >3.0 (Table 1). Despite profound differences in crown structure and physiology, the largest individuals of the other four tallest species also develop deep crowns (Table 1). Each of these species can produce *emergent* trees – large trees in dominant canopy positions above neighboring vegetation with crowns exposed to extremes of sun and wind. Interacting processes at leaf, branch, and whole-crown scales contribute to emergent crown development.

Trees make many leaf-level adjustments to maximize carbon gain. Since leaves reach photosynthetic saturation at a fraction of full sunlight, trees adjust leaf angles to minimize excessive heat loading and water loss (Duncan, 1971; Hikosaka and Hirose, 1997). Long-lived trees have constantly changing crowns and reiterate (resprout) following disturbance to restore leaf area (Smith and Brewer, 1994; Ishii and Ford, 2001). Within-crown growth produces leaves in newly illuminated regions, effectively maximizing productivity of the individual tree (Monsi and Saeki, 1953; Falster and Westoby, 2003). Leaves of many species are also phenotypically plastic, allowing them to vary widely in size, shape, and tissue density (Poorter et al., 2009; Oldham et al., 2010), expressed as leaf mass per unit area (LMA).

In tall crowns, leaves aggregate at the shoot level, shoots aggregate at the branch level, and branches are dispersed vertically at the tree level in response to *penumbral effects* (Anderson, 1964; Miller and Norman, 1971). Penumbral effects occur as the sun leaves a conic region of full shadow (*umbra*) behind an object that tapers into a region of diffuse shadow (*penumbra*) of useable light (Horn, 1971; Smith et al., 1989). The umbra, which is too dark for positive net photosynthesis, is minimized behind small objects such as leaves and shoots, because refracted light quickly illuminates behind them. On cloudy days, when diffuse light comes from all sides, the umbra is nearly eliminated. Aggregation of leaves at multiple scales effectively minimizes the umbra to relatively small regions directly underneath branches (Van Pelt and Sillett, 2008). We refer to the combined influences of phenotypic plasticity, aggregation at multiple scales, and crown reorganization as *crown optimization* (*sensu* Coomes et al., 2012), a phenomenon occurring to some extent in all trees. All long-lived species that also grow tall have the potential to develop an emergent crown.

1.2. Plot-level implications of emergent trees

During the lengthy process of crown optimization, abundant opportunities are created for other species to add leaf area in various canopy positions along the vertical gradient (Canham, 1988; Ishii et al., 2004). Diverse architectures and strategies of leaf display allow many trees, shrubs, and other plants that can grow in deep shade to exploit diffuse light (penumbra) in forest understories (Pickett and Kempf, 1980; King, 1994; Van Pelt and Franklin, 2000). Higher total leaf area due to shared canopy space by multiple species is termed *light-use complementarity* (hereafter LUC), which is a potential contributor to forest diversity and productivity (Ishii et al., 2013). Emergent trees maintain a high plot-level leaf area by growing deep crowns with larger, but fewer individuals. Vertical reorganization of foliage in large trees releases horizontal space and through LUC may increase total leaf area along the way – a process we call *emergent facilitation* (Fig. 1). Demonstrating emergent facilitation requires detailed, spatially explicit leaf area data from all species present. In tall, old-growth forests, these data must cover long distances (at least 3 times dominant tree height – Kuiper, 1988; Van Pelt and Nadkarni, 2004) to capture the full range of horizontal variability present in the forest.

Detecting LUC resulting from emergent facilitation might require considering forests as a collection of discrete, developmental units. Horizontal diversity in old-growth forests includes canopy gaps, regeneration patches, zones of dense trees, snags and logs, as well as sections with emergent trees (Richards, 1952; Franklin et al., 1981). In primary (old-growth) tropical rainforests, a *silvatic mosaic* is defined as a collection of *eco-units* (i.e., distinct patches with a similar internal structural and developmental trajectory following disturbances) and is the minimum landscape surface encompassing the full spectrum of horizontal diversity (Oldeman, 1983, 1990). Eco-units in the oldest forests consist of *structural ensembles* – cohorts of trees stratified vertically (e.g., understory, middle canopy, upper canopy). The largest trees define both the eco-unit and the

Table 1
Data from comprehensively mapped trees with the largest crowns of the six tallest species. Numbers reported are the highest leaf masses ever directly measured, come from trees with similar crown shapes, yet different in structure, genetics, and shade-tolerance.

Family	Taxa	Largest subset of mapped trees						
		Largest tree (Mg)	Leaf dry mass (kg)	*N*	Mean crown depth (m)	Mean crown diameter (m)	Depth to diameter ratio	Age range (years)
Cupressaceae	*Sequoia*	425[a]	>900	20	69.9	22.5	3.2	1120–2040
	Sequoiadendron	550[a]	>900	10	60.3	20.5	3.0	1200–3240
Pinaceae	*Pseudotsuga menziesii*	158[b,c]	>300	8	56.4	15.6	3.6	600–720
	Picea sitchensis	152[b]	>300	6	56.2	17.6	3.2	265–330
Myrtaceae	*Eucalyptus regnans*	215[d]	>400	4	60.7	18.9	3.2	210–430
	Eucalyptus globulus	230[b]	>400	2	61.9	19.7	3.1	250–400

[a] Sillett et al. (2015a).
[b] S.C. Sillett and R. Van Pelt (unpublished data).
[c] Van Pelt and Sillett (2008).
[d] Sillett et al. (2015b).

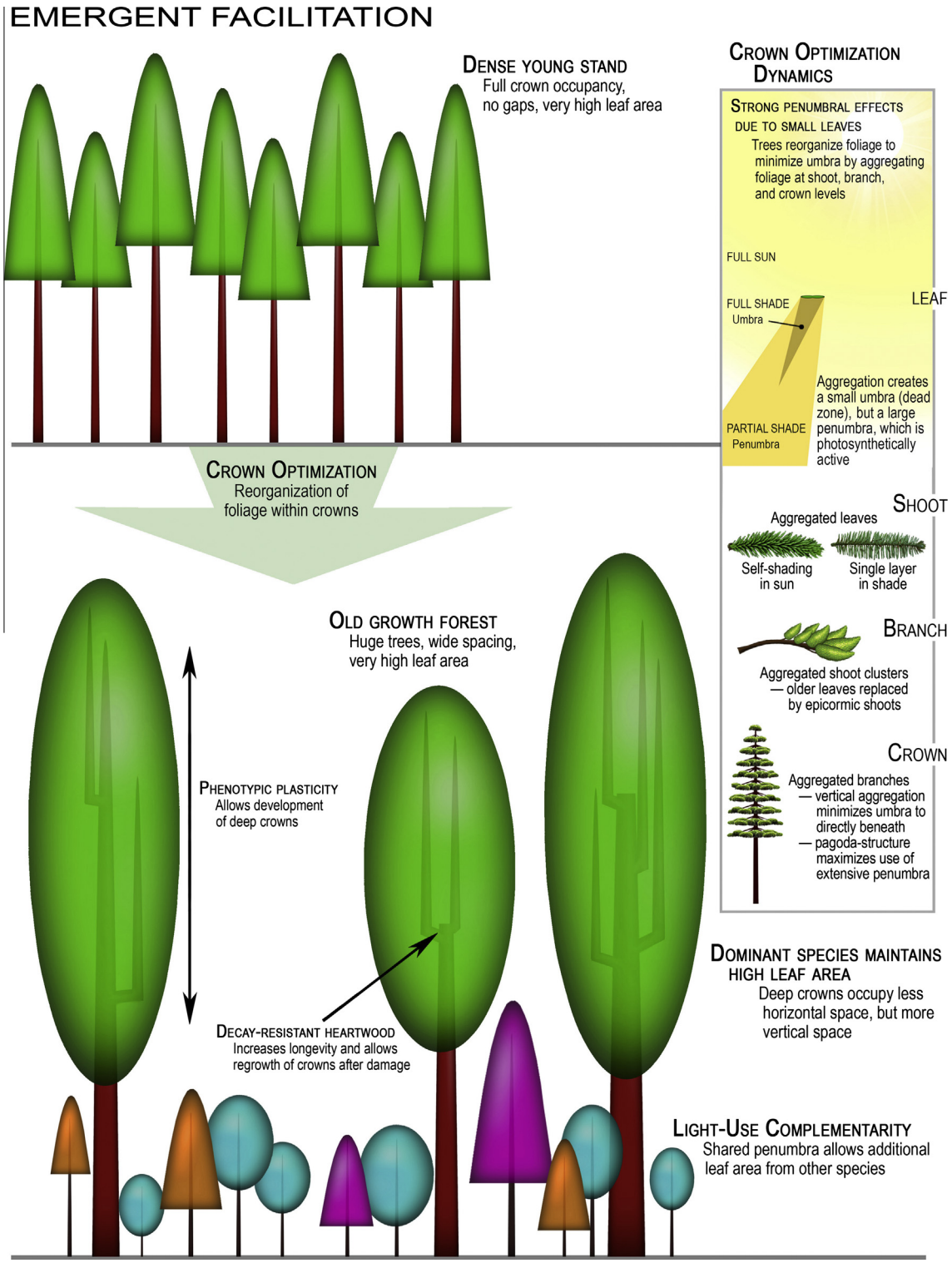

Fig. 1. Emergent facilitation. Becoming an emergent tree requires phenotypic plasticity. Crown optimization ensures reorganization of foliage to maximize photosynthesis through aggregation at multiple scales. Developing and maintaining an emergent crown requires decay resistance and the ability to reiterate after damage. The centuries it takes to develop trees with emergent crowns results in wide horizontal spacing between emergent trees, which thus provides available light for shorter species.

uppermost structural ensemble and have a strong influence over the other ensembles. Whether trees can become emergent or not depends in part on the species and in part on the structural context of neighboring trees. As trees age, damage from crown breakage and subsequent decay can lead to tree death and the degeneration of structural ensembles (Oldeman, 1990). If defined by canopy height, structural ensembles might be identifiable using remote sensing technologies such as aerial LiDAR (Lefsky et al., 1999; Kane et al., 2011). Further, if ensembles are defined by tree structure, and leaf area of all species within plots is quantified spatially, contributions of emergent trees to the forest as a whole can be determined.

1.3. Study system and objectives

Unique among the tallest species, some *S. sempervirens* (hereafter *Sequoia*) forests were intact throughout the Holocene such that they are much older than the oldest individual trees (Sawyer et al., 2000). In the rainforest (i.e., northern) part of its range, individual *Sequoia* reach heights >115 m and ages >2500 years (Sillett et al., 2015a). Unlike many tree species, where severe damage to a dominant tree crown initiates overall decline (Oldeman, 1990), decay resistance, reiterative capacity, and shade tolerance allow *Sequoia* to recover leaf area and expand its crown following disturbances (Sillett et al., 2015a). Eventually such trees become emergent with deep and highly individualized crowns (Fig. 2). These tree-level attributes, in part, allow *Sequoia* forests to achieve biomass exceeding 3000 Mg ha^{-1} (Westman and Whittaker, 1975; Fujimori, 1977; Sillett and Van Pelt, 2007).

The geographic range of *Sequoia* is limited to the west coast of North America where maritime conditions interface with a Mediterranean climate of hot, dry summers and cool, wet winters (Sawyer et al., 2000). A strong north-south precipitation gradient exists across the *Sequoia* distribution, influencing fire regimes (Fritz, 1932; Veirs, 1982; Lorimer et al., 2009). Variability in biomass and leaf area among these forests is poorly understood, and this deficiency is especially apparent with respect to abundance of dead wood. In northern rainforests, dead wood accumulations along streams range from 100 to 1800 Mg ha^{-1} (Keller et al., 1985), and in nearby terrestrial forests range from 210 to 580 Mg ha^{-1} (Graham, 2009). These values are far higher than reported for any other forest type (Harmon et al., 1986). The range of *Sequoia* also extends south into a much warmer and drier part of coastal California, where chaparral is the dominant vegetation (Stephens and Fry, 2005). Fire exerts major influence on the structure of *Sequoia* forests in this region, reflected by both smaller trees and lower quantities of woody debris (Lorimer et al., 2009; Sillett et al., 2015a).

Our primary goal is to better understand the processes by which *Sequoia* forests achieve global maxima and to elucidate the effect of emergent trees on forest structure. We pose three questions: (1) Does emergent facilitation lead to LUC in *Sequoia* forests? (2) Are emergent trees essential to achieving maximum leaf area at the plot level, or can maxima be reached with different forest structures? (3) Given the strong precipitation gradient with latitude, how do aboveground carbon and abundance of dead wood vary across old-growth *Sequoia* forests in California?

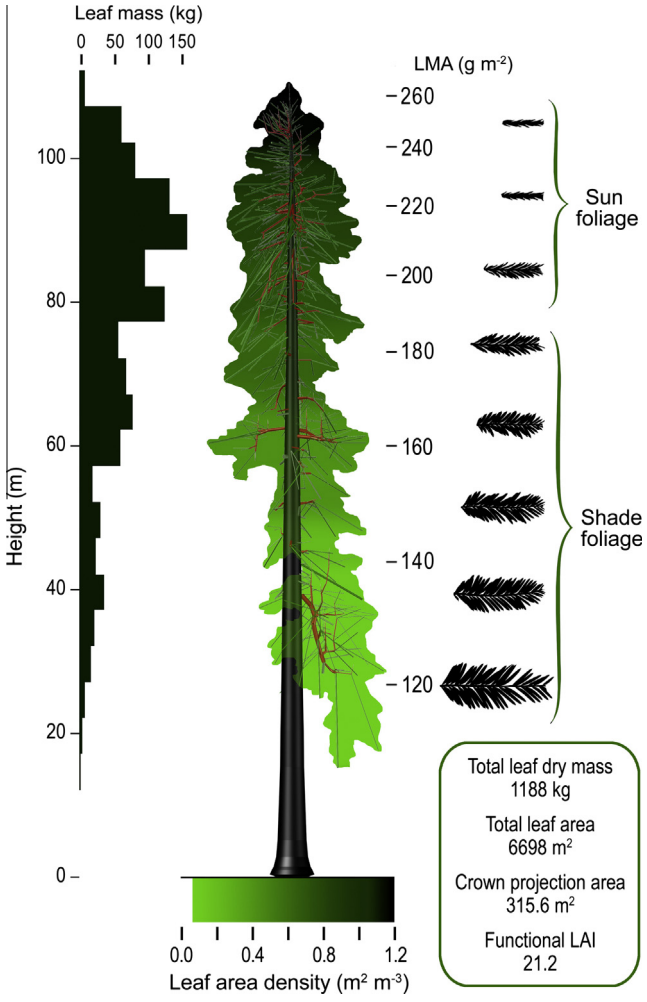

Fig. 2. Structure of an emergent tree. Few species express phenotypic plasticity of leaf form as dramatically as *Sequoia* (LMA changes >2-fold, *right*). Note that while lower crown is composed of shade foliage (*center*), it only represents about a quarter of leaf mass (*left*). Depicted tree structure is AutoCAD rendering of crown dataset for tree in RNP-low plot, which shows many branch and limb systems recovering from previous crown damage and regrowth. Silhouette generated from crown dataset, LiDAR point cloud, and photos.

2. Materials and methods

2.1. Approach

We used LiDAR data to select intact old-growth forests that included locally tall *Sequoia* throughout its range in California (Carroll et al., 2014; Sillett et al., 2015a). This allowed us to examine patterns in biomass, leaf area, and dead wood over a broad geographic area in the context of a strong precipitation gradient. In order to detect LUC, we needed spatially explicit plant-level biomass and leaf area over long enough distances to quantify horizontal variability within the silvatic mosaic. We installed 1-ha plots built around a centerline that was at least 315 m long, which made each centerline scaled 3 times the dominant tree height or longer. Since the centerline was so long, it was oriented to include at least two locally tall trees. Plot width was designed to ensure that any tree whose crown crossed the centerline was included in the plot, including leaning trees, making the plot at least 30 m wide. These values were increased to 316.23 × 31.62 to make each plot a full hectare that was 10 times longer than wide. While all eleven plots contained emergent trees, the 10:1 ratio of plot size was designed to capture horizontal variability of these tall forests and not emergent trees per se.

All aboveground vegetation within plots, including logs, stumps, and snags, was quantified in a spatially-explicit manner. Total dry masses of wood, bark, and leaves, as well as surface areas of cambium, bark, and leaves were computed for each plant via allometric equations for all dominant tree, shrub, fern, and herbaceous species. Historically, leaf area index (LAI), expressed as the projected area of leaves over a given area of ground, was difficult to quantify in tall forests for two reasons. First, species-level equations were inadequate to estimate the largest individuals present, or such equations did not exist. Second, optical methods for predicting LAI could not distinguish species and were plagued by issues of conversion accuracy associated with complex canopy structure (Asner et al., 2003; Olivas et al., 2013 – Bréda, 2003 has a thorough review of ground-based methods for measuring LAI). We considered the allometric approach more accurate and either made new equations for commonly encountered species or sought published equations for uncommon or minor species.

2.2. Study area

Plots were located in old-growth forests spanning a range of nearly 6 degrees of latitude across a wide precipitation gradient

(Fig. 3, Table 2). In the northernmost part of the range, *Sequoia* forests contain other tree species common in coastal sections of the Pacific Northwest – *Picea sitchensis*, *Thuja plicata*, and *Tsuga heterophylla*, which have their southernmost range limit at nearly the same location (Fig. 3). We used aerial LiDAR data from each location to quantify canopy height, crown structures, and terrain (Table 2).

Some of the most extensive old-growth *Sequoia* forests occur near the northern end of its range. Among the largest and most intact of these is the 3600 ha **Jedediah Smith Redwoods State Park (JS)** near Crescent City, California. Established in 1929 and later expanded, nearly the entire park is old-growth forest, although it does contain areas of relatively small-stature forests growing on ridges and areas recovering from fire. The 1360 ha of forest having trees >90 m tall includes some of the largest individual trees known (Van Pelt, 2001; Sillett et al., 2015a). With this location and the two that follow, *Sequoia* occupies nearly all geomorphic surfaces, so *upland* and *lowland* plots were established in each forest (shortened to 'up' and 'low' hereafter).

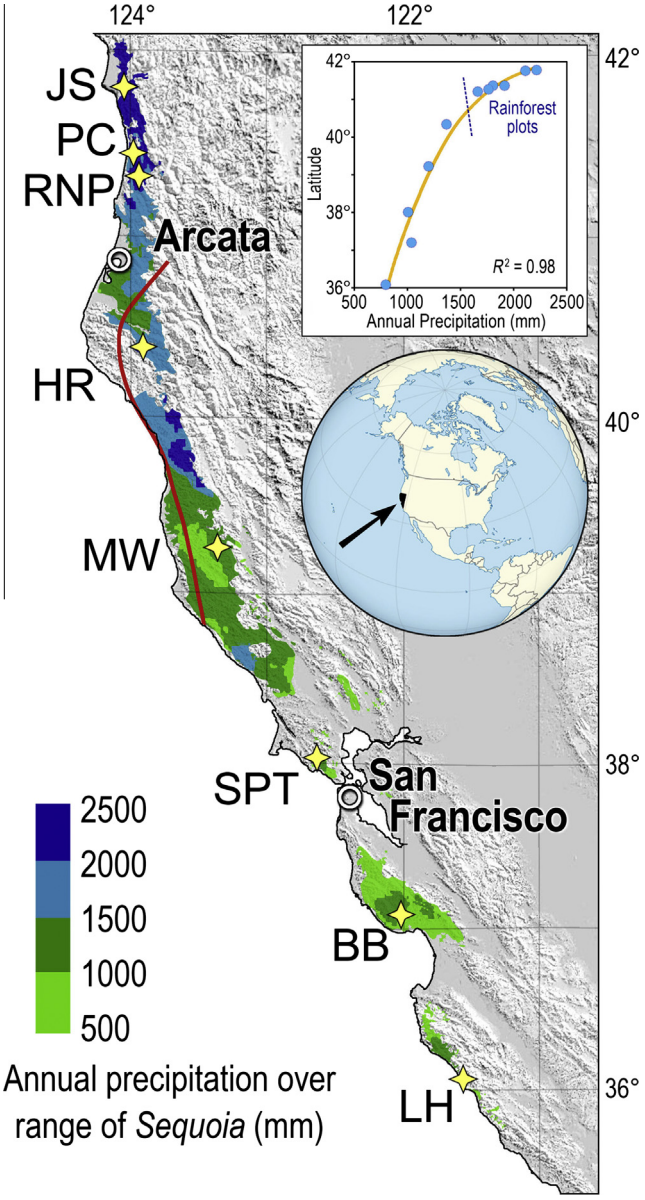

Fig. 3. Plot locations along the California coast. Colored areas indicate geographic range of *Sequoia sempervirens*, shaded by amount of precipitation. Red line represents southern/eastern limit of *Sequoia* associations with three Pacific Northwest tree species – *Picea sitchensis*, *Thuja plicata*, and *Tsuga heterophylla*. Top inset shows strong relationship between latitude and annual precipitation. Precipitation data from PRISM Climate Group (2012). Range map digitized from Griffin and Critchfield (1972). (For interpretation of the references to color in this figure legend, the reader is referred to the web version of this article.)

Prairie Creek Redwoods State Park (PC) is a 5300 ha reserve situated along the ocean just 34 km south of JS. Protected in the early 1920s and later expanded, the park is similar to JS in being nearly all old-growth forest. PC has 1760 ha of forest with trees >90 m (the largest single area remaining), which also contains several of the largest known individual trees (Van Pelt, 2001; Sillett et al., 2015a). Both JS and PC's proximity to the coast makes them exposed to winter storms that damage tree crowns, but subsequent growth and recovery of *Sequoia* creates some of the largest and most complex tree crowns (Sillett and Van Pelt, 2000; Sillett et al., 2015a).

Redwood National Park (RNP), which currently occupies 26,700 ha of the lower Redwood Creek drainage, was an area of intense logging during the mid-20th century. The discovery of tall trees in the early 1960s led to park establishment in 1968 followed by expansion in 1977. Even though the park is large, 85% of the old-growth forest was logged and much of the remaining 880 ha of forest with trees >90 m occur in widely scattered fragments. Unlike JS or PC, the drainage is protected from ocean storms, allowing trees to grow taller – these fragments contain a dozen trees >110 m tall, including the tallest and oldest known living *Sequoia* (Sillett et al., 2015a).

Sixty km south of Arcata, CA is **Humboldt Redwood State Park (HR)** and Rockefeller Forest – named for the benefactor whose contribution to the Save the Redwoods League led to its protection in 1929. The relatively narrow swath of tall forest along Bull Creek and lower South Fork Eel River has Earth's tallest canopy, containing ~80% of all known trees >107 m tall and >30 trees >110 m tall in 344 ha of alluvial river terraces. Even though the park is <100 km south of RNP, it is both farther inland and drier. Tree heights drop precipitously upslope of alluvial terraces, where *Sequoia* dominance quickly gives way to other genera, especially *Pseudotsuga* and *Notholithocarpus* with *Quercus* and *Arbutus* becoming common on south-facing slopes and ridges.

Old-growth *Sequoia* forests south of HR are more limited in extent primarily due to historical logging with a few exceptions. Thirty km from the ocean and at 283 m elevation, **Montgomery Woods State Natural Reserve (MW)** occupies a unique landscape position typically supporting dry forests and woodlands. The geophysical history of this location includes an ancient landslide that created a swamp along a valley bottom, providing *Sequoia* access to plentiful water, in addition to ample sunlight and protection from wind. Consequently, these conditions allow MW to achieve a higher tall tree density than even Rockefeller Forest with 15 trees >107 m tall occurring in a 9.4-ha patch of swamp forest.

Samuel P. Taylor State Park (SPT) is 21 km northwest of San Francisco Bay (38° latitude) and has the tallest trees in the region, which includes the nearby and heavily visited Muir Woods National Monument. The limitations of installing a plot with low human impact at the same time as locating plots throughout the latitudinal range of the species made SPT a key reference point. The area includes abundant *Notholithocarpus* and *Pseudotsuga* (some very large), and the normally scarce *Torreya californica* is fairly common.

The Santa Cruz Mountains are rugged, low-lying, and just south of San Francisco Bay, where *Sequoia* dominance extends to ridgelines in many areas. **Big Basin Redwoods State Park (BB)**, established in 1902, is California's oldest state park and located in the heart of this region. Current park boundaries contain 820 ha of old growth with large *Pseudotsuga* frequently co-occurring with *Sequoia*. Less than a dozen trees >90 m tall occur in the park.

Table 2
Summary of site characteristics. Precipitation and temperature data are annual averages for period 1895–2012 (PRISM Climate Group, 2012). Sites 1–6 are rainforests.

Plot	Location		Latitude (°)	Elevation (m)	Slope (%)	Aspect	Establishment date	Proximity to ocean (km)	Precipitation[a] (mm)		Temperature (°C)		LiDAR data sets	
									Annual	Summer	Winter T_{min}	Summer T_{max}	Flight date	Density (points m^{-2})
1	JS	Up	41.78	94	22–55	SW–NW	September 2010	5.2	2108[b]	68	3.5	22.4	2007	11.1
2		Low	41.77	80	0–33	E–S	November 2009	6.0	2215	69	3.2	23.2	2007	13.1
3	PC	Up	41.37	113	15–38	SW–NW	June 2011	5.2	1914[b]	55	2.5	21.9	2007	12.3
4		Low	41.36	58	0–13	W–NW	August 2011	4.7	1801[b]	54	3.2	20.2	2007	10.9
5	RNP	Up	41.26	158	28–80	N–SE	September 2009	5.0	1759	51	3.0	20.5	2007	17.0
6		Low	41.20	47	0–18	W–NW	October 2009	9.2	1663	46	3.5	20.6	2007	10.7
7	HR		40.34	50	0–8	SE–SW	August 2010	30.1	1369	27	4.1	24.5	2007	15.2
8	MW		39.23	283	0–4	SW–NW	November 2010	30.2	1196	15	2.0	29.3	2009	21.4
9	SPT		38.02	77	26–88	N–E	October 2011	7.9	1005	9	5.2	26.7	2010	8.0
10	BB		37.19	327	6–18	S–SW	December 2009	12.4	1039	14	6.3	26.9	2010	3.3
11	LH		36.09	167	23–100+	E–S	November 2011	2.0	801	5	3.9	23.1	2011	16.7

[a] Does not include interception from fog and other condensation, which can add 20–30% (Ruth, 1954; Harr, 1982).
[b] Drainage directly exposed to open ocean.

South of Monterey Bay (36.8° latitude), the steep Santa Lucia Mountain Range stretches for 170 km directly along the ocean, and *Sequoia* is largely restricted to deeply incised canyon bottoms. Three large state parks (Andrew Molera, Pfeiffer Big Sur, and Julia Pfeiffer Burns) and several smaller ones contain much of the old-growth *Sequoia* forest in the area and are heavily visited. Our southernmost plot at **Landels-Hill Big Creek Reserve (LH)** is even further south and occurs in the closed watershed of Big Creek at 36.1° latitude. This is the only known location south of Monterey Bay with *Sequoia* up to 80 m tall. Ridgelines and south-facing slopes have various mixtures of open chaparral with abrupt transitions to forest.

2.3. Plot measurements

2.3.1. Stem map creation

At each location, a centerline was established first by stretching fiberglass tapes down the plot center over its entire length (316.23 m). Within each plot, complete inventories were made of all live trees ⩾5 cm in diameter at breast height (BH – measured at 1.37 m) as well as all dead trees (snags and stumps) ⩾5 cm and taller than 0.5 m. Live trees were identified to species, tagged, and mapped for *X*–*Y* position on either side of the centerline using a compass and survey laser to measure the distance to the center (side) of each tree. Values along the tape served as a temporary *X* axis, later adjusted to slope-corrected horizontal distances. The *Y* value was a slope-corrected distance from the centerline to a reflector held at the side of the tree in line with the center. Trees on slopes or leaning trees required use of a compass to ensure reflector was held even with pith at ground level and parallel to tape. This procedure was often repeated on both sides of the trunk for large-diameter or complex trees. Once all trees were tagged and *X*–*Y* position recorded, hard copies of the initial stem map were brought into the field so they could be error-checked and updated while performing subsequent tasks. At least two additional updated versions of stem maps were error-checked via hard copies during subsequent visits.

Measurements of height, height to crown base, diameter at tag, and tag height above both high and low points of ground were collected for each tree (Table 3). Four crown radii were measured on each tree in cardinal directions, and large trees had four additional subcardinal measurements. Height to crown base was defined as the height at which the crown extends around at least one third of the trunk's circumference. If the tree or snag had a broken top, diameter was either measured or visually estimated, and height to the highest leaf was measured separately.

Measuring accurate tree heights in the world's tallest and densest forests offered several challenges. In the end, four methods were employed to measure tree height: (1) using a measuring tape lowered from the top of the tree, (2) vertical distance laser shots from a known height in a tree with a tape measure stretched from top to bottom and later corrected for base height differences, (3) sine method (*sensu* Larjavaara and Muller-Landau, 2013) with survey laser, and (4) extracting tree heights from LiDAR point clouds. Since plot installations and LiDAR flights were sometimes separated by a year or more, these were largely used as a check against our measurements of tree height. Methods 2 and 4 required establishing an exact link between tree locations and real Earth coordinates derived from a hybrid digital elevation model (DEM) created from LiDAR point clouds and ground surveys (see Appendix A for details on creation of the hybrid DEM).

Smaller trees, shrubs, ferns, herbaceous vegetation, and fine woody material were subsampled along plot centerlines (Table 3). Shrub plots were a 10% sample (1.58 m on either side of centerline) for the entire plot length for all shrubs ⩾50 cm tall and trees <5 cm DBH yet ⩾50 cm tall. We also used the centerline to establish 1-m-diameter circular plots for an inventory of understory vegetation as well as trees and shrubs <50 cm tall. Circular plots were spaced at 4-m intervals to take advantage of understory spatial independence within Pacific Northwest old-growth forests at this scale (Spies et al., 1999), yielding about 80 understory plots per centerline.

2.3.2. Crown volumes

Simple shapes were used to convert measurements of crown depth and crown radii into volumes. Paraboloids were used for *Alnus*, *Umbellularia*, and most conifers. The smaller/younger *Pseudotsuga* trees ($N = 33$) were also modeled as paraboloids, but the larger/older trees ($N = 19$) were modeled as 2/3 ellipsoids (Van Pelt and North, 1999). *Sequoia* was a special case that required a more complex approach described elsewhere (Sillett et al., 2015a), which provided a smoothly varying transition from paraboloids for small trees to ellipsoids for the largest trees. All other trees and shrubs were modeled as 1/2 ellipsoids.

$$\text{Paraboloid} = \frac{\pi}{2} \cdot CrD \cdot R^2 \quad 2/3 \text{ Ellipsoid (ellipsoidal equivalent)} = \pi \cdot \frac{3CrD}{4} \cdot R^2$$

$$\text{Ellipsoid} = 1/2 \text{ Ellipsoid} = \frac{4\pi}{3} \cdot \frac{CrD}{2} \cdot R^2$$

where *CrD* is crown depth and *R* is mean crown radius.

Table 3
Summary of measurements collected at each plot.

Structure	Category	Sample	Measurements						
Trees	Live ⩾5 cm DBH[a]	Main plot (10,000 m^2)	Species	X, Y location	*f* DBH	Height	Height to crown base	4–8 crown radii	Vigor
	Dead ⩾5 cm DBH[a]	Main plot (10,000 m^2)	Species	X, Y location	*f* DBH	Height	Estimate top diameter		
	Live <5 cm DBH, but ⩾50 cm height	Shrub transect (1000 m^2)	Species	X, Y location	Basal diameter				
	Live <50 cm height	Vegetation plots (64.4 m^2)	Species	Tallied					
Shrubs	Live ⩾10 cm basal diameter[b]	Main plot (10,000 m^2)	Species	X, Y location	Basal diameter	Height	Crown height	Average crown diameter	
	Dead ⩾10 cm basal diameter[b]	Main plot (10,000 m^2)	Species	X, Y location	Basal diameter	Height			
	Live ⩾50 cm height/length	Shrub transect (1000 m^2)	Species	X, Y location	Basal diameter				
	Live <50 cm height	Vegetation plots (80 ± 5, 1 m D)[c]	Species	Tallied					
Logs	Small end diameter ⩾30 cm	Main plot (10,000 m^2)	Species	X, Y location	End diameters[d]	Length	Decay class		
	Small end diameter <30 cm, but ⩾5 cm	Line intercept (316.2 m)	Species	X intercepts	Diameter at intercept		Decay class		
Ferns	Live	Vegetation plots (80 ± 5, 1 m D)[c]	Species	Percent cover	Dominant height				
Herbs/bryophytes	Live	Vegetation plots (80 ± 5, 1 m D)[c]	Species	Percent cover					

[a] Tagged at 1.4 m or top of buttress.
[b] Tagged at base.
[c] Vegetation plots are 1 m diameter circles spaced 4 m apart along the 316 m center line of each plot.
[d] One or more midpoint diameters were collected for long logs.

Leaf mass was not equally distributed within crowns—a cubic meter of crown volume at the top of a tree in full sun had a higher leaf dry mass than a cubic meter much lower in the crown (Fig. 2). We used our inventory of branch-mapped trees (Van Pelt and Sillett, 2008; Sillett et al., 2015a, R. Van Pelt and S.C. Sillett *unpublished data*) to estimate leaf mass distribution within crowns. Individual branch leaf masses of 54 *Sequoia*, 84 *Pseudotsuga*, and 28 *Tsuga* (including young, mature, and old, as well as vigorous and suppressed trees) were segmented into 5-m-height intervals based on crown depth. Fifth order polynomial curves were fitted to smoothed leaf mass distributions of each tree to generate a simplified pattern of vertical leaf mass distribution (Appendix B). Average curves were then scaled to the measured crown depth of each tree, and total leaf mass was partitioned into each 5-m-height bin based on the proportion of mass under the curve.

2.3.3. Tree base mapping and functional diameter

The buttressing influence of roots and other irregularities (e.g., fire scars) extended higher off the ground on larger trees, and with some trees >600 cm in diameter, the top of buttressing on flared lower trunks extended >10 m above the ground. In addition, due to the reiterative capacity of *Sequoia*, basal sprouts were common. Many of these fused into clusters of trees as they grew, and large tree clusters were highly irregular at ground level. Large trees, whether solitary or part of a cluster, usually required additional measurements due to the complexity of their bases. Buttressing, burn cavities, sprouting, and other anomalies rendered simple diameter tape measurements (tape wraps) inadequate, so we employed a number of techniques to quantify these structures. *Footprint mapping* involved generating cross sections of trunks at multiple heights and compiling sets of cross-sections to construct 3D models of non-round portions where trees emerged from the ground. The various methods used to generate 3D models of tree bases are described in Appendix C. The area of each cross section was converted to a *functional* diameter (diameter of a circle with equivalent area), which was then used with conic formulae incorporating the distance between cross-sections to calculate quantities of bark and wood (Sillett et al., 2015a). We defined functional diameter at BH as *f*-DBH, which was calculated for all *Sequoia*, because it was needed for use in allometric equations (Sillett et al., 2015a).

2.3.4. Decay in live trees

We excluded fire cavities and broken tops from trunk volumes, but unmeasured decay associated with these injuries resulted in lower wood densities that had to be addressed before calculating final trunk masses. Non-destructive internal scanning of large-diameter trunks was impractical, so we used published mill records following old-growth *Sequoia* logging and their reports of decayed unmerchantable timber. In a sample of 495 *Sequoia* trunks from the northern 400 km of the range, 336 (68%) had at least some decay (Kimmey and Hornibrook, 1952; Kimmey and Lightle, 1955). Basal wounds, fire cavities, and broken tops were the primary regions of decay. Older wounds had greater decay, but heartwood decay usually did not extend to reiterated trunks. Northern rainforests had the highest percentage of unmerchantable timber in old trees (34% in the furthest north – 42°), falling to 19% at the southern part of the study at 38.5° (Kimmey, 1958). However, the definition of unmerchantable varied with timber values and costs of cutting, hauling, and milling wood, and it encompassed more than just amount or degree of decay.

To hedge against uncertainties of unseen wood decay in standing trees we doubled the measured dimensions of wounds or cavities and calculated mass based on *Sequoia* dead wood Decay IV (Appendix D) as a proxy for the resulting decayed volume, because this type of wood lacked structural integrity. Estimated vertical extent of decay for trees with broken tops was assigned a value five times the broken top diameter, and a paraboloid extending down from the top was assigned the lower density. The Kimmey et al. samples revealed that smaller trees without wounds rarely had decay and that decay was largely limited to the tree base, so we designated a paraboloid of decay five times

taller than wide for all *Sequoia* >2 m *f*-DBH. We defined the volume of this paraboloid such that there was 1 m of sound wood surrounding a partially decayed core. For example, a tree with 4 m *f*-DBH with no external signs of decay was assigned a paraboloid of decay 2 m wide at the base and 10 m tall. In the old study, 20% of measured trunks had no decay, and decay in the other 80% was highly variable (Kimmey and Lightle, 1955), so we assigned these basal paraboloids the density of *Sequoia* Decay III, which retains some structural integrity.

2.3.5. Dead wood

The plot centerline was used to inventory logs <30 cm diameter with the line intercept method (Brown, 1974). Larger pieces of dead wood in forests can account for up to 90% of total mass (Sohn et al., 2013), yet their spatial extent is extremely variable (Harmon et al., 1986; Harmon and Sexton, 1996), so a 100% inventory of logs >30 cm diameter was added to each hard copied stem map initially as sketches. These were then scanned and used to update stem maps. With new maps in hand, each log was revisited and checked for location, diameter, and length. Any deviations were corrected by measuring distance and azimuth to known tree location(s) for both log ends. Dense and extensive fern glades often made log detection difficult, so during subsequent phases an additional search was conducted for large-diameter wood not previously mapped. The end diameters of each log were measured with longer logs receiving 1–3 additional diameter measurements. Heavily decayed logs as well as shards and other irregularly shaped pieces required two perpendicular diameter measurements to derive elliptical cross-sections. Tip-ups and other tree base features were mapped individually with height, width, and depth of the root plate recorded. Hollows and other features that reduced volumes of mapped pieces were also measured. We identified species and assigned a decay class to each piece of mapped woody debris.

The widely used 5-point classification system for log decay based on *Pinaceae* in the Pacific Northwest (Triska and Cromack, 1980) was adjusted for *Sequoia* to better account for its more decay-resistant heartwood. According to the original classification, Decay I and II logs were based on indicators of branch condition, sapwood decay, and bark sloughing, and Decay IV and V logs represented progressive stages degrading wood integrity. Large *Sequoia* logs, however, can persist in Decay III for many centuries before reaching Decay IV. During much of that time, if the log was not hollow, its heartwood was solid or at least a higher density than indicated by the outer surface. We designed a new, diameter-based decay classification to better account for this situation in *Sequoia* (Appendix D).

End diameters and lengths of each piece of woody debris were used for volume calculations. Straight sections of logs were modeled as conic frusta with either circular or elliptical cross-sections. Long logs often had multiple decay classes present, so these portions were separated prior to calculating mass. For logs that included the original tree base, wood density was reduced with the same paraboloid method used for standing trees to account for additional decay. Intercept data for logs <30 cm diameter were separated into groups based on species, decay class, and 5 cm diameter intervals (Harmon and Sexton, 1996). Each group's intercept length was expressed as a proportion of total intercept length and used to compute cylinder length. The mid-point diameter of each group was then used to calculate cylinder volume.

2.3.6. Linking local and remote data sets

Once installed, each plot had a relative coordinate system with no geo-referencing. Tall, dense *Sequoia* canopies made precise geo-location challenging. Accuracy depended on the number of GPS satellites detected by the receiver's antenna, but even survey-grade GPS units often recorded unacceptable location errors of several meters. Aerial LiDAR flights over each plot (Table 2) using a scanning laser mounted in an aircraft using a Global Positioning System (GPS) receiver for accurate positioning and an Internal Measurement Unit (IMU) for precise orientation aided geo-location. The resulting LiDAR data consisted of many individual laser pulse reflections from the forest, each with 3D coordinates. Data acquisition specifications constrained absolute geographic accuracy of point coordinates to <0.5 m, relative accuracy to <0.2 m, and resolution to <1 cm. The LiDAR point cloud was first used to create three primary 2.5D datasets (i.e., one Z value per X–Y pair): (1) a bare earth Digital Elevation Model (DEM), which is a model of the ground surface elevation; (2) a Canopy Surface Model (CSM), which is a model of the uppermost canopy surface elevation; and (3) a Canopy Height Model (CHM), which is the difference between the two and is a measure of canopy height. Details of how we created these are in Appendix A.

The initial LiDAR-based DEM recorded many topographic features on the forest floor only vaguely. High canopy densities created near-ground shadows (holes) in the point cloud, some of which were quite large (Fig. 4A and B). Interpolation of the remaining detectable bare ground DEM points attempted to fill the holes (Fig. 4C). A resulting artifact was that features such as rock outcrops and steep stream banks were smoothed or rounded. Ground-based laser surveys of each plot overcame these problems and captured all unusual and subtle topographic features, especially streams. Results from the ground-based laser surveys were scaled by the initial LiDAR-based DEM to create a hybrid with higher accuracy and precision than either alone (Fig. 4D, Appendix A).

2.3.7. Real Earth coordinates

Converting relative plot coordinate systems into real Earth coordinates was a multi-stage process. We used hours-long GPS track logs collected during plot installation to locate plot corners on the CHM. Once plot installation was complete and map layers were prepared, we used two additional datasets to locate plot boundaries more precisely than using the hybrid DEM alone (Fig. 4E). Because LiDAR point clouds yielded 3D models, the CHM represented a perfect orthographic view of the canopy. Ground-based measures of crown projections thus provided additional information for linking plots to real Earth coordinates (Fig. 5). Mapped logs evident in near-ground LiDAR point clouds provided another link (Fig. 4B). A minimizing algorithm was finally used to refine corner point locations calculated from all data sets to an exact rectangular 316.23 × 31.623 m plot whose border was converted to Universal Transverse Mercator coordinates. Errors in corner point locations were ±0.2–0.5 m for plots on flat ground and 0.4–0.8 m for plots on steeper terrain. Once ground-based data sets were linked to LiDAR, all stems and footprint maps were assembled on hybrid stem maps along with snags, logs, and water features (Fig. 6), and real Earth coordinates were calculated for the base and top of every tagged tree.

2.4. Plant processing for allometric equations

Our approach to quantifying aboveground attributes of standing trees via crown mapping, hierarchical sampling, and subsequent dissections for biomass was developed during studies of several tall species (Van Pelt et al., 2004; Van Pelt and Sillett, 2008; Sillett et al., 2010, 2015a,b). Here we used this approach to quantify additional species growing with *Sequoia*, including trees, shrubs, ferns, and other non-woody plants. We developed allometric equations that can be applied in any old-growth forest throughout the range of *Sequoia* and for much of the Pacific Northwest as well. Detailed tree mapping leading to whole-tree quantity estimations was done for

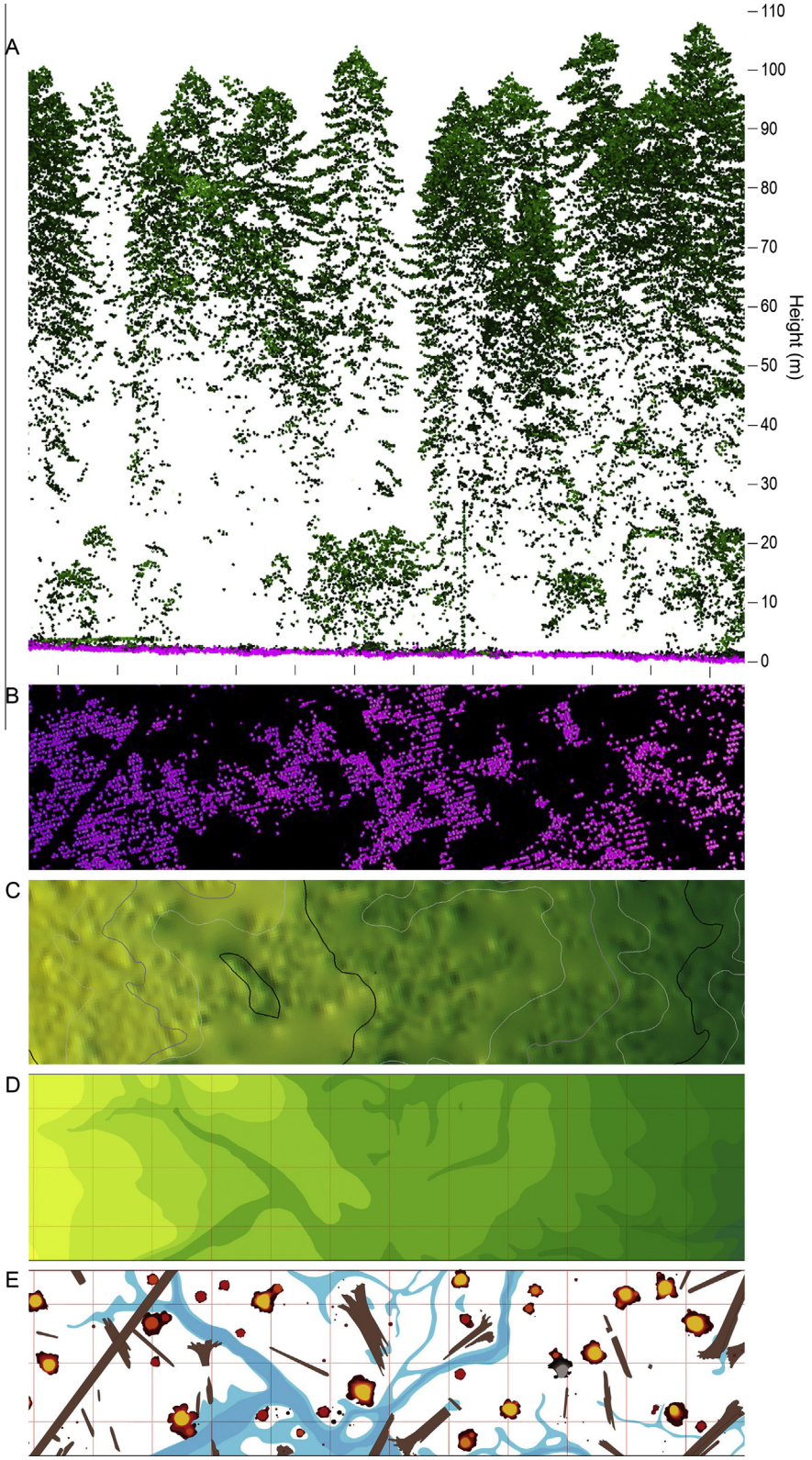

Fig. 4. LiDAR point cloud links stem map to real Earth coordinates, part 1. (A) depicts portion of canopy profile at MW (LiDAR height scale in m). Pink dots in (A) and (B) are ground returns used to create DEM. (C) depicts initial DEM at 0.25-m contours. Additional field mapping used to create final DEM in (D). Logs evident in ground returns (B) also used to link final stem map (E) to real Earth coordinates, if present. Note that large holes in near-ground returns created by dense crowns (B) make interpreting streams problematic without additional survey work. (For interpretation of the references to color in this figure legend, the reader is referred to the web version of this article.)

Sequoia (N = 97, Sillett et al., 2015a), *Pseudotsuga menziesii* (N = 115), *T. heterophylla* (N = 44), *Acer macrophyllum* (N = 23), *Acer circinatum* (N = 27), *Alnus rubra* (N = 58), and *Notholithocarpus densiflorus* (N = 118). Similarly, shrub dissections leading to whole-plant equations were done for *Rubus spectabilis* (N = 25), *Vaccinium ovatum* (N = 30), and *Vaccinium parvifolium* (N = 41).

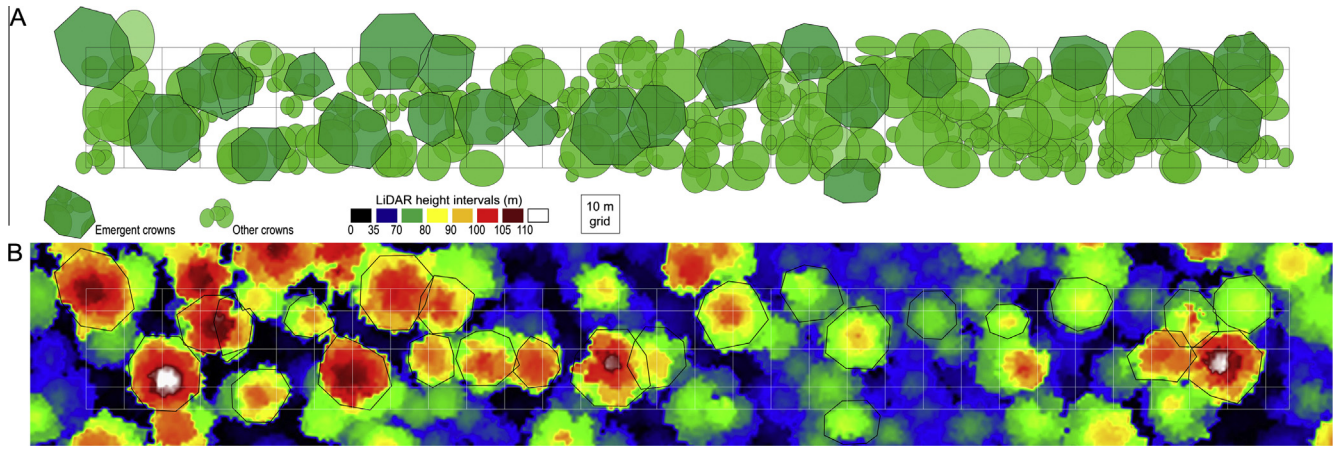

Fig. 5. LiDAR point cloud links stem map to real Earth coordinates, part 2. (A) depicts ground-based measurements on crown projections of 425 live trees at RNP-up. Emergent trees shown as octagons derived from crown radius measurements. Other trees had four crown radii measured in cardinal directions, each of which defined an ellipse. (B) shows crown projections of emergent trees fitted to LiDAR CHM as an additional tool used to convert relative scale of original map to real Earth coordinates.

New allometric equations for the ferns *Athyrium felix-femina* (N = 14% cover plots), *Blechnum spicant* (N = 22% cover plots), and *Polystichum munitum* (N = 45% cover plots) were also prepared, as well as the herbaceous *Oxalis oregana* (N = 30% cover plots). Details of how each of these were sampled, processed, and analyzed are found in Appendices E–K.

In summary, we produced 180 new equations – 105 of these are new whole-plant equations for predicting total wood, bark, and leaf dry mass, bark and cambium surface area, projected leaf area, and total leaf number for 11 species of trees and shrubs as well as additional equations to predict leaf mass of three fern species and *Oxalis* (Appendix L). For multi-step calculations using intermediate estimates, the standard error (SE) was carried forward at every step, so that final reported SE contains all sources of error (e.g., SE for leaf area on a single tree includes error for predicting whole-tree leaf mass, as well as error converting leaf mass to area). All of these new allometric equations can be used throughout old-growth forests of the Pacific Northwest and the California coast. Biomass equations for minor woody plants and herbaceous plants other than *Oxalis* were obtained from published sources (Smith and Brand, 1983; Alaback, 1986; Means et al., 1994; Halpern and Lutz, 2013).

Dried and ground samples of leaves, bark, sapwood, and heartwood of *Sequoia* were analyzed for carbon content (% dry weight) using a CHNOS Elemental Analyzer (Elementar, Hanau, Germany) at the Center for Stable Isotope Biogeochemistry, University of California, Berkeley, USA. Percent carbon values for most of the other dominant components of biomass were obtained from the literature (Appendix M). For shrub or herb components where species-level equations were unavailable, we used values from similar species in the Rocky (Jain et al., 2010) or Appalachian Mountains (Moore et al., 2007).

2.5. Quantifying horizontal diversity

2.5.1. Centerline analyses

Once all leaf areas were calculated, plot centerlines were analyzed, meter by meter, for all contributing leaf area in a 1 m^2 cylinder above each – a total of 3476 calculations for 11 plots. Shrubs and small trees were measured in a continuous transect down plot centerlines, so their leaf area contributions were scaled and shared among each centerline meter as their proportional crown diameters indicated. Similarly, trees whose crowns overlapped the centerline had leaf areas partitioned into 1-m^2 parcels based on crown projections, and parcels were assigned to the appropriate centerline cylinder intersecting each crown. This assumed leaf area was equally distributed throughout the crown projection, or equally in azimuth, which may not always be the case. However, an analysis from mapped tree inventories for *Sequoia*, *Pseudotsuga*, and *Tsuga* (N = 166) confirmed the curve for tree-level leaf area versus distance from main trunk was relatively flat with depressions at main trunk and crown edge. Since our crown radius measurements ignored outlier branch extensions, we modeled the curve as flat. Ferns and other non-woody plants were sampled every 4 m down plot centerlines, so values for each sampled meter were extended to neighboring 1-m^2 parcels.

2.5.2. Quantifying influence of emergent trees

We designed seven complementary indices based on spatially explicit information to determine if emergent trees promote LUC. At the plot level, simple metrics that isolated the influence of emergent trees were mean crown mass (i.e., whole tree dry mass – main trunk dry mass), mean crown volume, and their standard deviations. A plot with emergent trees produced a mean and standard deviation (SD) greater than those for otherwise similar plots lacking such trees. Since some plots had abundant regeneration while others did not, and we were interested in comparing the distribution and abundance of large trees, plot-level metrics that treated all trees equally overwhelmed important patterns. By examining only *Sequoia* for the seven indices and by ignoring stems smaller than 20 cm *f*-DBH, we eliminated most of this concern without substantially affecting plot-level basal area (0–0.7% reduction among 11 plots), leaf area (0–2.2%), or mass (0–0.3%) totals.

High mean individual crown mass or volume relative to other plots indicated many emergent trees since these forests had more smaller and fewer larger trees. The standard deviation of crown mass or volume, however, reflected the full spread from very small to very large. Since all plots had some small trees, if the plot had a few emergent trees, the SD would be relatively high compared to others. Crown mass and volume were correlated, so we created two plot-level indices out of the four possibilities that included mean and SD: (Index 1) mean crown mass, and (Index 2) SD of crown volume.

Emergent trees were also detected by skewness of plot-level leaf mass or area, as the presence of these trees skewed the median when leaf area was sorted high to low. Index 3 was the leaf mass of the median tree – the tree where the sum of leaf area for all *Sequoia* larger than it had a value no smaller than the sum of all *Sequoia* smaller than it. A related metric also derived from sorting by size was a count of how many large trees it takes to reach a sum of half

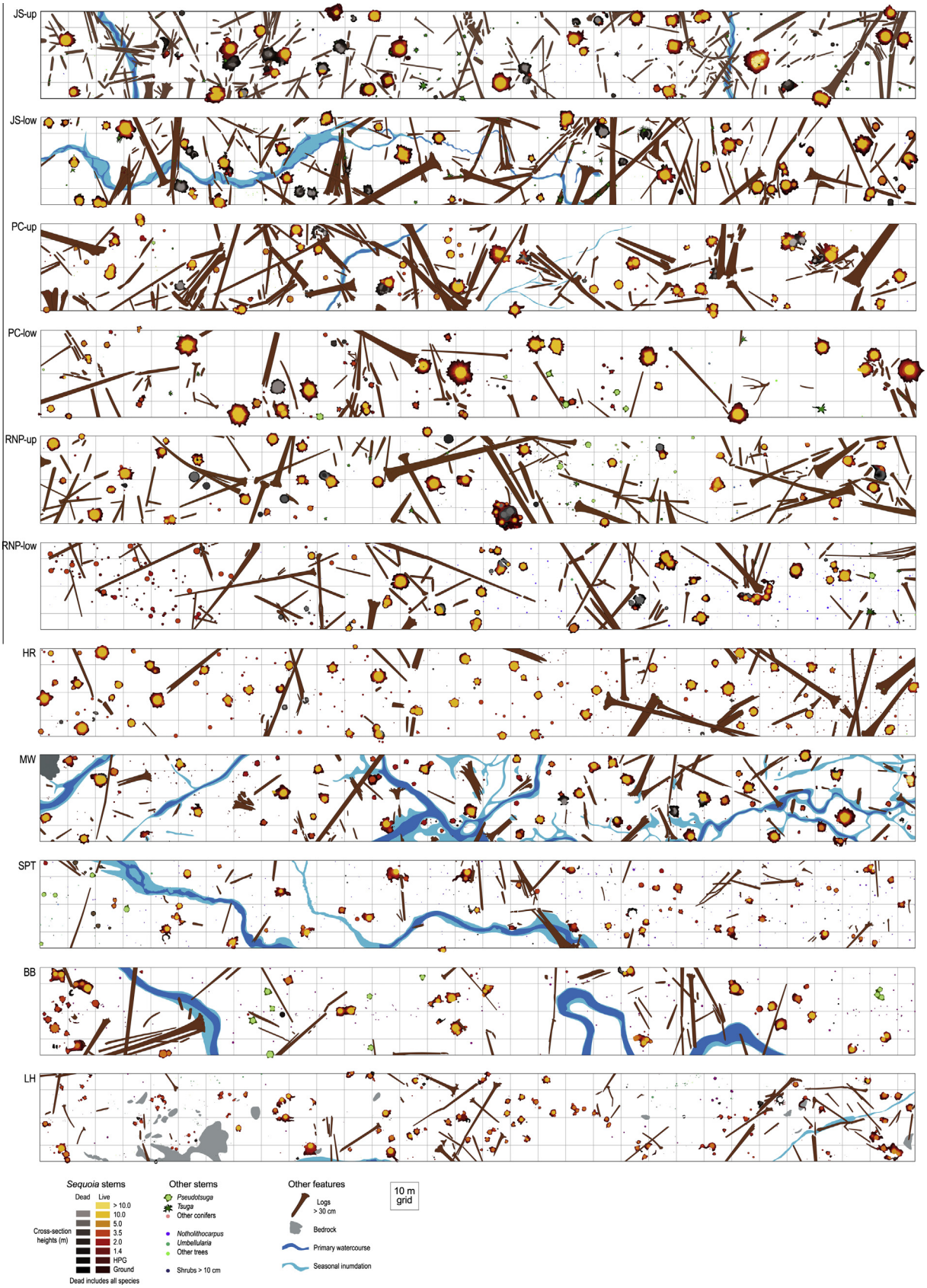

Fig. 6. Stem maps of eleven plots from north to south. First six panels are northern rainforest plots. Complex tree clusters and tree castles are visible in most of the plots. Abundance of woody debris in these plots may make it appear trees fall frequently but bulk of this material is Decay III, and thus very old wood.

the total *Sequoia* leaf area (Index 4). This was an indicator of number of emergent trees, since if the plot had trees with emergent crowns, the count to get half of the plot-level leaf mass or area was relatively small. Noteworthy, Index 4 was simply a count and so independent of tree size. Plots with emergent trees were also easily detectable using an analysis of the meter-by-meter centerline LAI with the strongest being SD of *Sequoia* LAI. Because emergent trees had high leaf areas yet were separated in space, the centerline LAI for a plot with emergent crowns had many large peaks and troughs and thus a very high SD (Index 5).

Characteristics of emergent trees were also detectable from the LiDAR CHM. At 0.75 of the CHM peak value (h_{max}), where crowns of tall trees were wide, emergent trees became large polygons, often consisting of a single crown. Lesser trees at this height either had a small polygon or none at all. Denser groups of tall trees did not have single-tree or paired polygons at this height but rather a polygon formed by multiple crowns. The first index to use the 0.75 h_{max} interval CHM was based on the fact that plots with emergent trees not only had large individual polygons (compared to those in a densely-packed plot), but they also had relatively consistent spacing. Thiessen polygons (also called Voronoi diagrams) defined regions of closeness to a set of points. Each polygon defined an area of influence around a point based on proximity to other points so that polygon boundaries were perpendicular to lines connecting pairs of adjacent points, whose lengths indicated spacing. With tree stem locations used as points, each polygon was analyzed to separate polygons at 0.75 h_{max} on the CHM into individual tree crowns and to compute tree–tree distances. The CHM beyond plot boundaries was used to extend polygons, so that all adjacent polygons had tree-to-tree distances calculated. All distinct polygons within each 1-ha plot were used for crown distance analysis and the creation of Index 6: mean tree–tree distance at 0.75 h_{max}. Our final metric of emergentness, Index 7, was also derived from the LiDAR CHM in that emergent trees were the only trees that still had a large diameter crown at the 0.75 h_{max}. All trees tall enough to contribute to the total 0.75 h_{max} polygon area were counted, and mean crown size was computed as 0.75 h_{max} polygon area divided by the number of contributing trees. Finally, a composite index, called the *emergent crown index* (ECI), was created by calculating the mean of the seven indices.

2.5.3. Structural ensembles

After the meter-by-meter centerline analysis of LAI and development of the ECI, our third approach for quantifying horizontal diversity used spatial information to define structural ensembles, which represented patches of differing forest structure. Just as plot width was designed to be at least 15 m from the centerline to include any tree whose crown may be directly overhead, a 15 m search radius was used to define a circular window that was moved along each centerline, meter-by-meter, to distinguish ensembles. Using the LiDAR point cloud, we constructed a *Relative Height*, *Canopy Height Model* (RH–CHM) scaled from 0 to 1 based on the tallest tree in each plot (see Appendix A). Within each window, all LiDAR-derived RH–CHM points were divided into 10 equal tiers with each tier representing 10% of h_{max}. Since our CHM was prepared at 0.5 m horizontal spacing, each moving window contained slightly >2800 points. We wanted to quantify leaf area of all species under the moving window, so this analysis began at centerline distance 15 m (radius of the window) and moved to distance 301 m (15 m from the plot end). Once assigned to an ensemble, that meter along the centerline was removed from further classification. The first ensemble, **Canopy Gap**, was defined as having 50% or more of the CHM values from the bottom three tiers (i.e., <0.3 relative height).

Despite its strengths, the LiDAR point cloud alone could not distinguish conifer species in *Sequoia* forests. *Pseudotsuga* (up to 97 m tall) and *Tsuga* (up to 83 m tall) grow among *Sequoia*, while *Sequoia*, *Tsuga*, and *Notholithocarpus* can all be abundant in understory and mid-level canopy positions. We used a 30-m-diameter moving window of species-level basal area congruent with the RH–CHM to define a second ensemble, **Shared Dominance**, where *Sequoia* shares dominance with other tree species (i.e., at least 20% of basal area derived from non-*Sequoia*). After removing both Canopy Gap and Shared Dominance ensembles, only *Sequoia*-dominated ensembles remained.

Former gaps, where large trees were removed through wind or fire and now refilling with young–mature trees, or where larger trees had recently fallen or been damaged in areas where smaller trees were already present, comprised the **Emerging Canopy** ensemble. This youngest and shortest of the *Sequoia*-dominated ensembles was often of limited extent and not present in all plots. Defining this ensemble was a two-step process. First, the moving window had to have <5% RH-CHM values in the top two tiers, ⩾60% RH-CHM values in the middle four tiers, and <20% RH-CHM values in the bottom two tiers. Second, we ran a 5 m smoothing spline of standard deviation of basal area to exclude large and old trees that may have been short or broken. This curve revealed large peaks at the inclusion/exclusion boundary for large trees, which provided clear demarcation points for selection. With these three ensembles now removed from the total, most of what remained contained the tallest portions of the RH-CHM.

The **Codominant Canopy** ensemble, which was common in all plots, was characterized by a nearly continuous canopy of very tall tree crowns. It was defined as the moving window having ⩾40% RH-CHM values in the top three tiers and <5% in the bottom two tiers. The **Emergent Crowns** ensemble was characterized by very tall trees with large crowns, yet widely spaced – leaving gaps in between that often extended to near ground level. It was defined as the moving window having ⩾20% RH-CHM values in the top three tiers and between 10% and 30% in the bottom two tiers. Any unused portions of centerlines remained unclassified. A dichotomous key was prepared (Appendix N) to clarify the above descriptions and facilitate comparisons among ensembles.

3. Results

3.1. Plot summary

A total of 4089 live trees ⩾5 cm *f*-DBH were mapped and measured in eleven 1-ha plots, including 1927 *Sequoia* and 455 standing dead trees. Tree height and *f*-DBH ranged up to 112.6 m and 681.2 cm, respectively, and several plot-level quantities were global maxima (Table 4). Trees >110 m tall occurred in three plots (RNP-up, HR, MW), trees >100 m tall occurred in seven plots (also JS-low, PC-up, PC-low, RNP-low), and trees >90 m tall occurred in all but the southernmost plot (LH).

Trees >1000 years old were found in all eight northern plots (Sillett et al., 2015a), and despite a limited sample for which we had age estimates, trees >1800 years old occurred in at least PC-low, RNP-up, and MW. Both SPT and BB had trees >600 years old, and the oldest trees sampled at LH were 330–390 years old. Details on individual *Sequoia* that were climbed, mapped, and aged as part of this study were published elsewhere (Sillett et al., 2015a).

All plots had trees >330 cm *f-DBH*, and all but three southern plots (SPT, BB, LH) had trees >450 cm *f-DBH*. The northernmost plot (JS-up) had 26 trees per hectare (TPH) > 300 cm, and 18 TPH > 400 cm, which exceed any previously reported values. Equally superlative was PC-low, which had *only* 14 TPH ⩾ 300 cm, but 12 of these were ⩾400 cm, seven were >500 cm, and four were ⩾600 cm, with the latter two details exceeding JS-up. Four other

plots had at least 19 TPH ⩾ 300 cm *f*-DBH. The densest plot was HR with 38 TPH ⩾ 200 cm *f-DBH*, and four other plots had at least 30 TPH ⩾ 200 cm *f-DBH*. Live tree basal area ranged from 160 to 461 $m^2\ ha^{-1}$ with seven plots having ⩾300 $m^2\ ha^{-1}$ of *Sequoia* alone (Table 4). JS-up had the highest value ever recorded for a single species (449 $m^2\ ha^{-1}$) as well as the record for standing dead trees in an intact forest of 115 $m^2\ ha^{-1}$.

Crown volumes of all vascular plants combined ranged from nearly 200,000 to over 450,000 $m^3\ ha^{-1}$. Three plots had *Sequoia* crown volumes >350,000 $m^3\ ha^{-1}$. Two of these plots were rainforests with emergent trees, one of which (RNP-up) also had the highest non-*Sequoia* crown volume. A third plot (HR) had 370,000 $m^3\ ha^{-1}$ *Sequoia* crown volume with virtually no contributions from other species. Even though tree size varied considerably along the north-south precipitation gradient, crown diameters of the largest trees were remarkably consistent (mean radius of 10 widest trees in all plots was 9.1 ± 0.1 m), so crown depth was the primary reason for the large crown volumes reported. Mean crown depth of the 20 largest trees was >55 m in all six of the northern rainforest plots, and <55 m in all the others. Interestingly, the latter includes the two tallest forests (HR and MW), whose average crown depth was relatively low due to prevalence of the Codominant Canopy ensemble.

3.2. Live biomass, leaf area, and aboveground carbon

Biomass partitioning by species and tissues is described in Appendix E and resulted in the development of many new allometric equations (Appendices F–K), which allowed separate computations of leaf, bark, and wood surface areas, volumes, and dry masses by species and plot for all important tree, shrub, fern, and herbaceous species. This was achieved with complete dissections or crown mapping of 765 individual trees and shrubs that included subsamples to get bark thickness, wood and bark density, SLA, leaf count, and carbon content. Dissections resulted in a summary of plot-level masses, by species or life-form, including standard errors of all predicted values (Appendix L).

Standing live biomass ranged from 1600 to 4530 Mg ha^{-1} with the eight northern plots all having >3000 Mg ha^{-1} (Appendix O). Most of this material was wood and bark of *Sequoia* trunks – three plots had >500 Mg ha^{-1} of *Sequoia* bark alone. *Pseudotsuga* provided the highest two non-*Sequoia* contributions to total aboveground live biomass, which were at BB (333 Mg ha^{-1} – 83% *Pseudotsuga*) and RNP-up (249 Mg ha^{-1} – 62% *Pseudotsuga*).

Leaf dry masses of nine individual *Sequoia* trees exceeded 1 Mg, five of which were in one plot (PC-low, Sillett and Van Pelt, 2007). Leaf masses ranged from nearly 16 to over 31 Mg ha^{-1} with seven plots having >20 Mg ha^{-1} of *Sequoia* leaves (Appendix O). Vertical distribution of leaf mass showed similar distribution patterns with peaks in leaf mass generally occurring at 50–70% of h_{max} (Fig. 7). Despite differences in total leaf mass, the peak 5 m height interval was similar among plots with values generally 2–2.5 Mg ha^{-1}. HR was the only plot with any *Sequoia* 5 m band exceeding 2.8 Mg ha^{-1}, and it had three – all adjacent and totaling 9.4 Mg ha^{-1} from 70 to 85 m. HR and MW had the highest total *Sequoia* leaf mass (25.7 and 24.9 Mg ha^{-1}), while simultaneously having the lowest non-*Sequoia* leaf mass (0.3 and 0.7 Mg ha^{-1}). The highest all-species total leaf mass, however, occurred in JS-up (31.4 Mg ha^{-1}), which also had the highest non-*Sequoia* contribution to leaf mass (11.2 Mg ha^{-1}, Fig. 7, Fig. 8 top). The understory fern *Polystichum* had the highest non-*Sequoia* leaf mass of any species, especially in the six rainforest plots, where leaf mass averaged 2.9 Mg ha^{-1} with a maximum of 5.1 Mg ha^{-1} (JS-up). After *Polystichum*, *Tsuga* had the next largest contribution to non-*Sequoia* leaf mass. It was present only in the six rainforest plots (mean 1.3 Mg ha^{-1}) and reached a maximum of 2.6 Mg ha^{-1} (JS-up). A large and old population of *V. ovatum* occurred in JS-up as well, which included 30 plants >10 cm basal diameter per hectare, and added 2.3 Mg ha^{-1} of leaf mass. Bryophytes growing on the forest floor, logs, and tree bases were also abundant in rainforest plots, where three of the four northernmost plots had bryophyte dry masses >200 kg ha^{-1} (Appendix O).

Overall plot-level LAI ranged from 9.9 to 19.4 with the eight northern plots all having LAI > 15.8 (Fig. 8 bottom). All eight of the northern plots had *Sequoia* LAI > 11, with the two tallest plots (HR, MW) having *Sequoia* LAI ⩾ 14 (Fig. 8 bottom). Total conifer LAI reached 15.9 in one plot (RNP-up), and >13.0 in six plots. *Polystichum* contributed substantially to leaf area in the six rainforest plots, four of which had LAI > 2.4 from this fern alone. *Oxalis*, which was abundant on the forest floor in all but one plot (SPT) and had 25–50% ground cover in five of the plots, contributed up to 1.3 LAI. Plot-level proportions of total leaf mass and area were similar (Fig. 8). The largest difference involved the herbaceous category and the presence of *Oxalis*, whose extremely thin leaves had SLA values 3–10 times higher than other species.

Dead wood mass in standing snags varied by more than an order of magnitude from 22 Mg ha^{-1} at the southernmost plot (LH) to nearly 300 Mg ha^{-1} at RNP-up (Table 5). While *Sequoia* comprised >95% of snag mass in eight plots, one plot (SPT) had 47.5 Mg ha^{-1} of dead *Pseudotsuga* and only 13.1 Mg ha^{-1} of dead *Sequoia*. PC-low also had a substantial standing dead *Pseudotsuga* component (34.7 Mg ha^{-1}), and nearly all of the 64.4 Mg ha^{-1} of *Sequoia* snag mass in this plot was contributed by one large individual. A huge two-trunked snag in another plot (RNP-up) with both portions >70 m tall and an individual dry mass of 195.7 Mg contributed the majority of total snag mass in that plot (295 Mg). Log mass was also variable with two of the fire-prone southern plots having <100 Mg ha^{-1}. Three of the rainforest plots had log masses >500 Mg ha^{-1} with the maximum (608.5 Mg ha^{-1}) consisting of >99% *Sequoia* heartwood (Table 5). This plot (PC-up) included bases and portions of eight fallen, non-hollow trees >250 cm *f*-DBH with the largest single piece (within plot boundaries) having a dry mass of 84.2 Mg. Log abundance depicted in Fig. 6 may appear that trees fall over frequently in the northern plots, but most of this material was decay-resistant heartwood from many centuries of accumulation and very little was newly fallen material in Decay I (Table 5). Despite idiosyncrasies of snag and log occurrence among the 11 plots, the precipitation gradient (800–2200 mm) explained 80% of variation in total dead wood mass.

Total aboveground dry mass exceeded 5000 Mg ha^{-1} in one plot and was ⩾4000 Mg ha^{-1} in seven of the eight northern plots (Fig. 9). *Sequoia* heartwood contributed the bulk of this mass, ranging from 61.5% (SPT) to 76.7% (JS-low) of plot totals. Seven plots had *Sequoia* heartwood mass >3000 Mg ha^{-1} (mean 3250 Mg ha^{-1} in rainforest plots) with the highest (3890 Mg ha^{-1}) occurring in the wettest two plots (JS). Non-*Sequoia* contributions (two blue categories in Fig. 9) were <5% in eight of 11 plots with one plot (BB) reaching 13.3%. In terms of total aboveground carbon, all but one of the eight northern plots had >2000 Mg ha^{-1} of carbon with the two northernmost and wettest plots (JS) having the highest (mean 2530 Mg ha^{-1} of carbon, Table 6). *Sequoia* bark alone contained more carbon than all other species combined in every plot except BB. *Sequoia* heartwood in snags, logs, and live trees was the primary reservoir of long-term carbon storage, and seven plots had at least 1500 Mg ha^{-1} of carbon in *Sequoia* heartwood with the two JS plots having the highest (mean 1930 Mg ha^{-1}). *Sequoia* heartwood percentages of total carbon ranged from just over 60% in dry, southern plots to nearly 80% in northern, rainforest plots.

Table 4
Tree characteristics by plot. Data are from the tagged population of trees only. Basal area and maximum diameter (Max D) were calculated from ƒDBH (see text). Values in red are global maxima.

Location	Tree type	Number of trees per hectare: Total	≥ 300 cm	≥ 200 cm	≥ 100 cm	Basal area (m^2)	Max D (cm)	Max Ht (m)	Crown Vol (m^3)
JS-up	*Sequoia sempervirens*	79	**26**	32	39	**448.7**	604.1	98.5	243,900
	Tsuga heterophylla	96			2	11.86	140.4	64.1	44,700
	Picea sitchensis	1				0.04	21.9	21.5	350
	Notholithocarpus densiflorus	2				0.01	9.3	5.0	111
	Rhamnus purshiana	5				0.07	18.9	15.0	760
	Vaccinium ovatum	29				0.37	22.3	6.8	980
	Sambucus racemosa	3				0.02	9.7	5.7	209
	Vaccinium parvifolium	1				0.02	14.7	4.3	18
	Acer circinatum	6				0.05	12.8	10.0	850
	Dead	44	5	11	21	**115.2**	468.7	48.1	
	Totals	266	31	43	62	**576.3**			
	Live only	222	26	32	41	**461.1**			291,900
JS-low	*Sequoia sempervirens*	77	19	36	48	382.4	591.8	108.3	276,000
	Tsuga heterophylla	88				7.02	93.4	50.8	36,260
	Notholithocarpus densiflorus	4				0.07	27.4	17.9	1100
	Rhamnus purshiana	2				0.02	12.1	10.5	137
	Acer circinatum	51				0.49	23.0	9.8	5270
	Dead	24	5	6	15	79.0	439.9	63.9	
	Totals	246	24	42	63	468.9			
	Live only	222	19	36	48	390.0			318,700
PC-up	*Sequoia sempervirens*	137	14	34	58	305.4	504.2	109.9	280,000
	Tsuga heterophylla	56				0.94	53.8	42.3	5220
	Pseudotsuga menziesii	1			1	0.93	108.8	66.7	1440
	Notholithocarpus densiflorus	3				0.06	23.8	14.4	345
	Rhamnus purshiana	20				0.16	22.1	12	1160
	Acer circinatum	2				0.01	6.3	5.7	62
	Corylus cornuta californica	6				0.05	11.7	8.2	380
	Dead	22	2	7	13	53.6	307.6	33.8	
	Totals	247	16	41	72	361.1			
	Live only	225	14	34	59	307.5			288,600
PC-low	*Sequoia sempervirens*	97	14	21	41	400.6	681.2	101.9	359,200
	Tsuga heterophylla	10			1	3.24	144.8	69.5	8230
	Pseudotsuga menziesii	7			6	11.55	193.6	82.2	12,040
	Umbellularia californica	10				0.74	51.0	20.0	2321
	Acer macrophyllum	5				0.88	71.7	28.8	7990
	Rhamnus purshiana	1				0.04	22.8	9.2	141
	Vaccinium ovatum	2				0.01	9.8	5.2	88
	Vaccinium parvifolium	1				0.01	9.9	3.9	41
	Dead	12	1	1	7	24.0	428.9	43.5	
	Totals	145	15	22	55	441.0			
	Live only	133	14	21	48	417.1			390,000
RNP-up	*Sequoia sempervirens*	164	19	28	49	310.6	491.6	112.6	**374,600**
	Tsuga heterophylla	162			2	7.48	104.8	55.5	33,510
	Pseudotsuga menziesii	28			3	10.23	186.9	77.1	28,080
	Abies grandis	7				0.83	59.3	51.5	3220
	Notholithocarpus densiflorus	45				1.34	52.5	27.5	12,880
	Alnus rubra	4				0.19	31.0	25.3	570
	Rhamnus purshiana	2				0.02	14.5	12.3	215
	Chrysolepis chryospylla	1				0.04	21.3	17.1	294
	Rhododendron macrophyllum	15				0.14	13.8	8.6	615
	Dead	43	5	9	12	74.2	404.2	76.7	
	Totals	471	24	37	66	405.1			
	Live only	428	19	28	54	330.9			**454,000**

RNP low	*Sequoia sempervirens*	171	9	27	64	268.1	504.1	108.6	274,200
	Tsuga heterophylla	16			1	2.66	122.0	57.7	6230
	Pseudotsuga menziesii	1			1	2.49	178.2	79.5	4500
	Notholithocarpus densiflorus	174				6.27	68.5	41.5	32,110
	Umbellularia californica	5				0.62	76.6	43.0	2420
	Alnus rubra	1				0.08	31.0	21.5	465
	Cornus nuttallii	1				0.01	10.0	7.0	22
	Rhododendron macrophyllum	12				0.05	11.9	8.0	336
	Dead	45		3	12	35.5	310.0	58.8	
	Totals	426	9	30	78	315.7			
	Live only	381	9	27	66	280.3			320,300
HR	*Sequoia sempervirens*	339	19	**38**	64	358.7	461.1	112.5	372,500
	Notholithocarpus densiflorus	2				0.01	8.3	6.5	50
	Umbellularia californica	2				0.04	18.5	15.4	523
	Acer macrophyllum	3				0.01	10.0	10.8	167
	Dead	29		2	7	18.0	250.0	43.1	
	Totals	375	19	40	71	376.8			
	Live only	346	19	38	64	358.8			373,200
MW	*Sequoia sempervirens*	284	21	33	68	351.4	479.5	111.6	329,200
	Dead	52		3	5	22.3	320.4	88.7	
	Totals	336	21	36	73	373.6			
	Live only	284	21	33	68	351.4			329200
SPT	*Sequoia sempervirens*	134	1	14	53	147.4	343.7	90.6	212,300
	Pseudotsuga menziesii	4			5	7.94	181.5	81.6	11,370
	Torreya californica	5				0.05	15.6	9.9	193
	Notholithocarpus densiflorus	214				3.64	56.5	30.5	21,180
	Umbellularia californica	26				0.82	56.5	24.8	3920
	Acer macrophyllum	3				0.15	41.1	11	1100
	Dead	89		2	6	17.9	235	50.7	
	Totals	475	1	16	64	177.9			
	Live only	386	1	14	58	160.0			250,000
BB	*Sequoia sempervirens*	139	8	24	48	196.8	358.9	90.2	178,600
	Pseudotsuga menziesii	10		1	10	21.02	207.7	78.4	35,990
	Notholithocarpus densiflorus	375				9.76	72.1	40.4	43,780
	Dead	28	1	1	6	17.9	320.0	17.7	
	Totals	552	9	26	64	245.4			
	Live only	524	8	25	58	227.6			247,000
LH	*Sequoia sempervirens*	306		8	76	175.0	331.1	79.3	180,000
	Notholithocarpus densiflorus	65				3.95	92.9	34.5	8900
	Umbellularia californica	94				1.46	56.4	18.3	6770
	Alnus rhombifolia	3				0.04	16.4	12.1	430
	Heteromeles arbutifolia	4				0.02	8.9	4.7	54
	Ceanothus cuneatus	11				0.05	10.9	7.1	585
	Dead	67			2	10.7	150.0	53.0	
	Totals	550		8	78	191.2			
	Live only	483	0	8	76	180.5			196,800

3.3. Centerline analysis of leaf area

When viewed on a meter-by-meter basis, leaf area distribution was extremely variable with dramatic spikes caused by emergent trees (Fig. 10 – darkest red colors). The 1-m-wide sample passed through several canopy gaps >15 m wide, but small gaps between large tree crowns were common, especially in the northernmost plots. Individual trees or tree clusters could carry immense leaf area – some individual m^2 cells exceeded an LAI of 30 – but were often separated by gaps extending to the ground. Also apparent (especially in rainforest plots) was the abundance of *Oxalis* and *Polystichum* in the understory. Emergent crowns were evident in most plots and most obvious at JS-up. While the centerline summary statistics in Fig. 10 represented only a 1-m-wide sample,

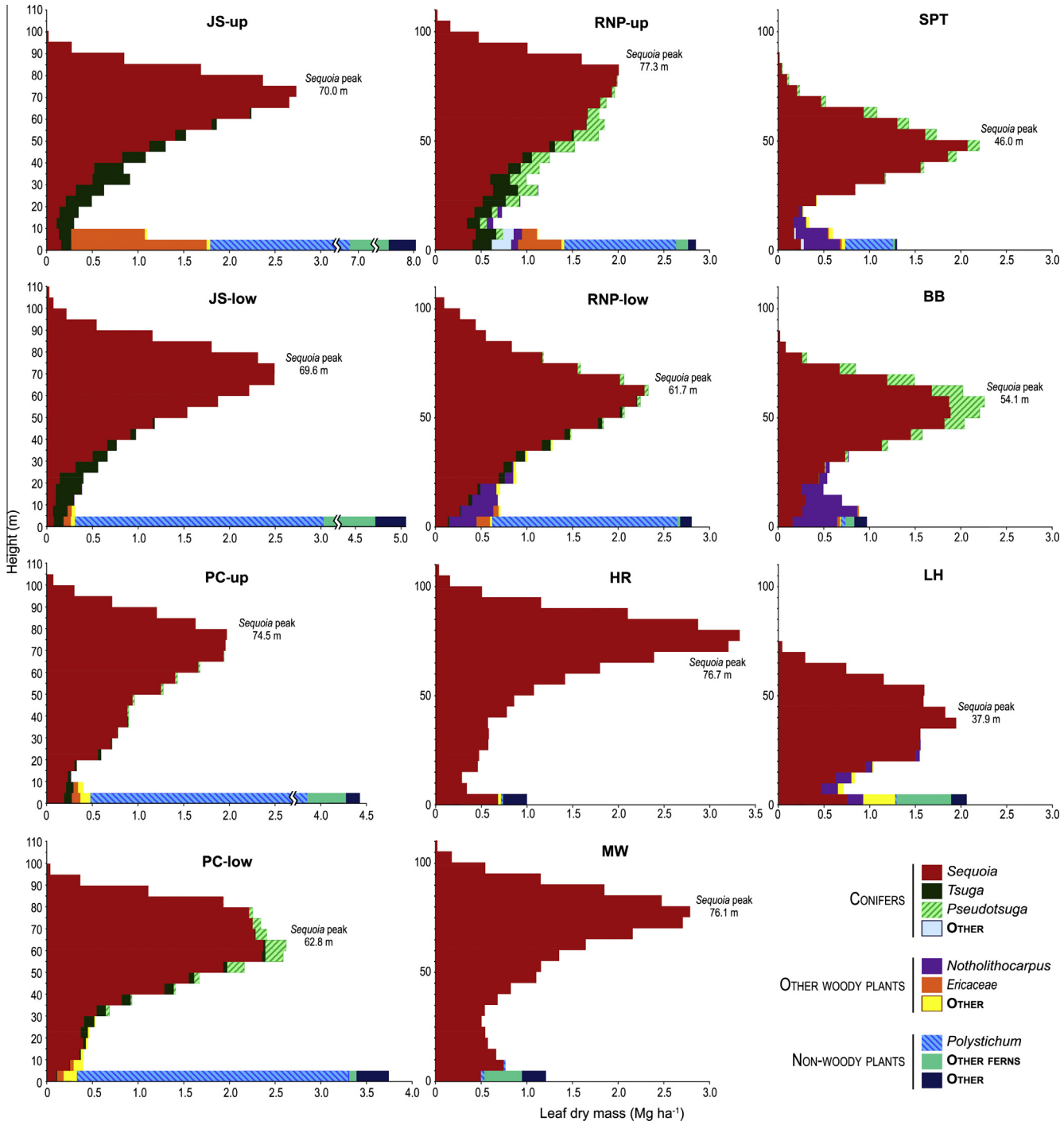

Fig. 7. Vertical distribution of leaf mass. Foliage from all life-forms partitioned into 5-m height bins using measured crown dimensions and allometrics. Note similarities but also subtle differences in *Sequoia* leaf mass distribution with strongest peaks occurring in HR and MW, both of which have relatively low understory masses. Also note high understory masses of rainforest plots.

mean centerline LAI was similar to plot-level LAI (Appendix O) with exception of BB, whose centerline passed through some large canopy gaps.

3.4. Detecting LUC with emergent crown indices

3.4.1. Plot-level metrics

The plot with 26 TPH > 300 cm *f*-DBH (JS-up) had the highest mean crown mass (Index 1) at 5.3 Mg, and PC-low was the only other plot to have mean crown mass >3.5 Mg (4.8 Mg – Table 7). Even though all trees <20 cm *f*-DBH were removed before this analysis, the mean crown mass for five of the plots was <1 Mg. Standard deviation of crown volume (Index 2) was highest in PC-low, which had 7 trees with crown volumes of 15,000 m^3 or more, two of which were >25,000 m^3. RNP-up was the only other plot with individual crown volumes >20,000 m^3 ($N = 2$ trees).

3.4.2. Individual tree metrics

When sorted by leaf area, the median crown mass (Index 3) was highest in two rainforest plots (JS-up, PC-low) at >10 Mg. The

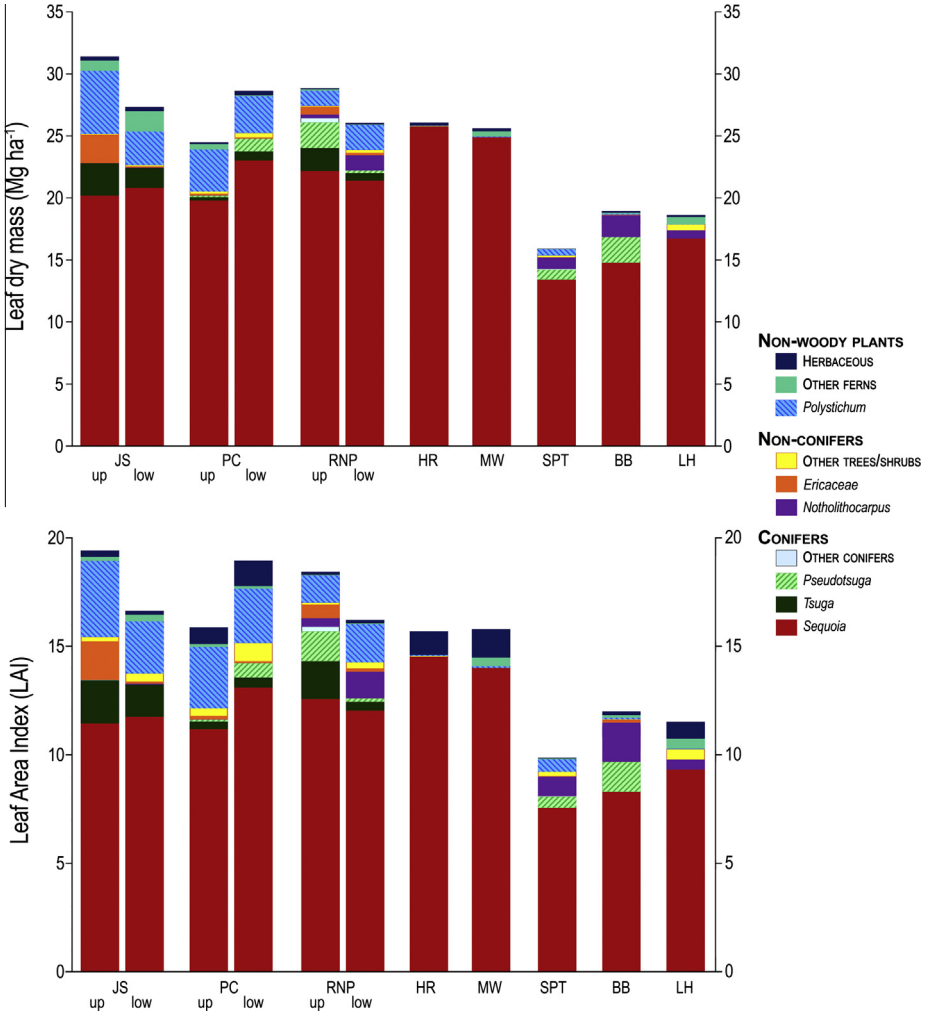

Fig. 8. Top panel uses stacked bars to condense data presented in Fig. 7. Lower panel depicts LAI partitioned identically to top panel. Six rainforest plots (left) show substantial contributions from other species. Note that thin leaves of understory plants such as *Oxalis* barely register in top panel but are prominent in lower panel.

skewness of this index was indicated by the next two highest plots having median crown masses of only 5–6 Mg and all remaining plots having median crown masses <3 Mg (Table 7). The same two rainforests (JS-up, PC-low) were the only plots where <15 trees were needed to reach half of plot-level LAI (Index 4).

3.4.3. Centerline variation

The SD of *Sequoia* LAI (Index 5), whose values were similar to means, had a maximum SD occurring at JS-up (13.9). Only JS-up and BB had SD greater than the mean. In JS-up, this was caused by regular spacing of 100 Mg trees with gaps in between. In BB this was caused by four dense clusters of trees separated by large gaps or *Pseudotsuga*. Another plot with SD of *Sequoia* LAI > 12.0 was RNP-low, which had 13 peaks with >30 LAI and two large gaps.

3.4.4. LiDAR metrics

Index 6 used tree-tree distances generated by Thiessen polygons for all crowns at 0.75 h_{max}. This was the only index where RNP-up scored higher than PC-low. Both plots were similar with few but very large, widely spaced polygons. This was also the only index where one of the southern plots scored high. The BB plot was more open than the others, but it also had trees with (relatively) large crowns, including contributions from nine mature *Pseudotsuga*. Index 7 was based on how many crowns contributed to the cross-sectional area at 0.75 h_{max}, and three plots (JS-up, PC-low, RNP-up) had mean emergent crown areas >70 m^2 with the maximum (92.8 m^2) occurring at PC-low. Remarkably, at 76 m above the ground, PC-low had 26 trees within a single hectare that had a mean crown diameter of 10.9 m.

3.4.5. Emergent Crown Index (ECI)

All seven indices comprising the ECI were positively and significantly ($P < 0.017$) correlated with non-*Sequoia*, non-conifer, and understory LAI. Index 1 (mean crown mass) and Index 4 (# of trees to reach ½ LAI) had the strongest relationship to non-*Sequoia* LAI (Table 7). However, ECI itself was the strongest correlate of all possible combinations of component indices. PC-low had the highest ECI (0.94), ranked highest on three of the seven indices, and ranked second-highest on three others. Similarly, JS-up had a very high ECI (0.90) and also ranked highest on three of the indices. Both plots had very large trees that were widely spaced – of 30 trees with the highest leaf mass among 11 plots, 16 were from PC-low and JS-up.

3.5. Demonstrating LUC using structural ensembles

The five structural ensembles occupied 85% of centerline distance (2671 m out of 3146 m total) using a 30-m-diameter moving window (Fig. 11). Based strictly on this classification, 116 different contiguous units of the five ensembles were identified,

Table 5
Summary of dead wood by log and snag categories. All values in Mg ha^{-1}. Note modest values for Decay I *Sequoia*, which are fallen trees from recent decades. Values in red are global maxima.

			JS-up	JS-low	PC-up	PC-low	RNP-up	RNP-low	HR	MW	SPT	BB	LH
LOGS	*Sequoia sempervirens*	Bark	0.04 ± 0.00	0.11 ± 0.00	0.06 ± 0.00	0.38 ± 0.02	0.11 ± 0.00	0.28 ± 0.01	0.08 ± 0.00	9.85 ± 0.77	0.01 ± 0.00	0.93 ± 0.06	0.78 ± 0.06
		Sapwood	4.1 ± 0.2	0.5 ± 0.0	3.8 ± 0.3	3.7 ± 0.1	2.4 ± 0.1	5.3 ± 0.3	14.6 ± 1.1	9.4 ± 0.7	0.5 ± 0.0	4.8 ± 0.3	10.0 ± 0.6
		Decay I	20.1 ± 0.4	71.8 ± 1.4	75.8 ± 1.5	13.7 ± 0.3	59.3 ± 1.2	20.0 ± 0.4	48.8 ± 1.0	69.3 ± 1.4	10.8 ± 0.2	39.1 ± 0.8	5.4 ± 0.1
		Decay II	30.7 ± 1.2	67.8 ± 2.7	90.3 ± 3.6	14.2 ± 0.8	72.0 ± 2.8	36.9 ± 1.4	84.8 ± 3.4	15.0 ± 0.6	8.8 ± 0.4	22.3 ± 0.9	25.8 ± 1.0
		Decay III	189.7 ± 9.2	309.4 ± 15.3	412.0 ± 20.3	65.6 ± 5.1	321.4 ± 16.0	176.4 ± 8.6	116.3 ± 5.7	96.4 ± 4.8	50.4 ± 2.5	73.4 ± 3.6	40.8 ± 1.9
		Decay IV	36.8 ± 2.0	73.6 ± 5.5	24.4 ± 1.6	20.0 ± 0.8	18.6 ± 1.3	15.7 ± 1.2	12.4 ± 1.0	11.8 ± 0.7	2.9 ± 0.2	1.0 ± 0.1	2.1 ± 0.1
		Decay V	13.3 ± 1.2	8.4 ± 0.9	2.0 ± 0.2	6.1 ± 0.9	6.4 ± 0.7	0.6 ± 0.1	0.0 ± 0.0	0.9 ± 0.1	0.1 ± 0.0	3.6 ± 0.4	0.0 ± 0.0
		Heartwood	290.7 ± 14.0	530.9 ± 25.8	604.6 ± 27.2	119.6 ± 7.9	477.8 ± 22.0	249.7 ± 11.8	262.4 ± 11.1	193.5 ± 7.5	73.0 ± 3.2	139.4 ± 5.7	74.0 ± 3.1
		Total	294.9 ± 14.2	531.5 ± 25.8	608.4 ± 27.5	123.8 ± 8.1	480.3 ± 22.1	255.2 ± 12.1	277.0 ± 12.2	212.7 ± 9.0	73.5 ± 3.3	145.1 ± 6.0	84.8 ± 3.8
	Abies grandis	Total					0.1 ± 0.0						
	Pseudotsuga menziesii	Total				23.6 ± 0.6	12.1 ± 0.8				8.9 ± 0.4	42.4 ± 1.5	
	Tsuga heterophylla	Total	22.5 ± 1.1	43.0 ± 1.5	0.1 ± 0.0	0.6 ± 0.0	4.7 ± 0.3	0.8 ± 0.0					
	Notholithocarpus densiflorus	Total					2.4 ± 0.1	17.2 ± 0.5			11.9 ± 0.4	5.4 ± 0.2	6.9 ± 0.2
	Umbellularia californica	Total				0.8 ± 0.0					1.4 ± 0.1		3.8 ± 0.1
	Acer macrophyllum	Total		0.9 ± 0.0		2.9 ± 0.1							
	Acer circinatum	Total		0.1 ± 0.0									
		LOG TOTAL	**317 ± 15**	**575 ± 27**	**608 ± 28**	**152 ± 9**	**500 ± 23**	**273 ± 13**	**277 ± 12**	**213 ± 9**	**96 ± 4**	**193 ± 8**	**96 ± 4**
SNAGS	*Sequoia sempervirens*	Heartwood	242.7 ± 7.9	188.7 ± 6.1	117.8 ± 3.8	64.4 ± 2.4	292.6 ± 7.3	121.2 ± 4.1	37.5 ± 1.0	85.0 ± 2.8	13.0 ± 0.4	25.3 ± 0.8	19.6 ± 0.7
		Total	242.9 ± 7.9	189.7 ± 6.1	117.9 ± 3.9	64.4 ± 2.4	294.1 ± 7.3	122.1 ± 4.1	38.1 ± 1.0	85.2 ± 2.8	13.1 ± 0.4	25.6 ± 0.8	21.7 ± 0.8
	Tsuga heterophylla	Total	21.0 ± 0.5	9.6 ± 0.3	3.2 ± 0.1	0.19 ± 0.01	0.57 ± 0.02	0.18 ± 0.01					
	Pseudotsuga menziesii	Total				34.7 ± 1.4	0.32 ± 0.01				47.5 ± 1.7	0.27 ± 0.01	
	Abies grandis	Total					0.01 ± 0.00						
	Torreya californica	Total									0.00 ± 0.00		
	Notholithocarpus densiflorus	Total					0.05 ± 0.00	1.13 ± 0.04			7.8 ± 0.3	0.88 ± 0.03	0.14 ± 0.01
	Umbellularia californica	Total									0.19 ± 0.01		0.29 ± 0.01
	Acer macrophyllum	Total				0.11 ± 0.00		0.20 ± 0.01			0.03 ± 0.00		
	Alnus rubra	Total					0.12 ± 0.00						
	Rhamnus purshiana	Total			0.02 ± 0.00								
	Corylus cornuta Californica	Total						0.00 ± 0.00					
	Heteromelies arbutifolia	Total											0.00 ± 0.00
		SNAG TOTAL	**264 ± 8**	**199 ± 6**	**121 ± 4**	**99 ± 4**	**295 ± 7**	**124 ± 4**	**38 ± 1**	**85 ± 3**	**69 ± 2**	**27 ± 1**	**22 ± 1**
		GRAND TOTAL	**581 ± 24**	**775 ± 34**	**730 ± 31**	**251 ± 13**	**795 ± 31**	**397 ± 17**	**315 ± 13**	**298 ± 12**	**164 ± 7**	**220 ± 9**	**118 ± 5**

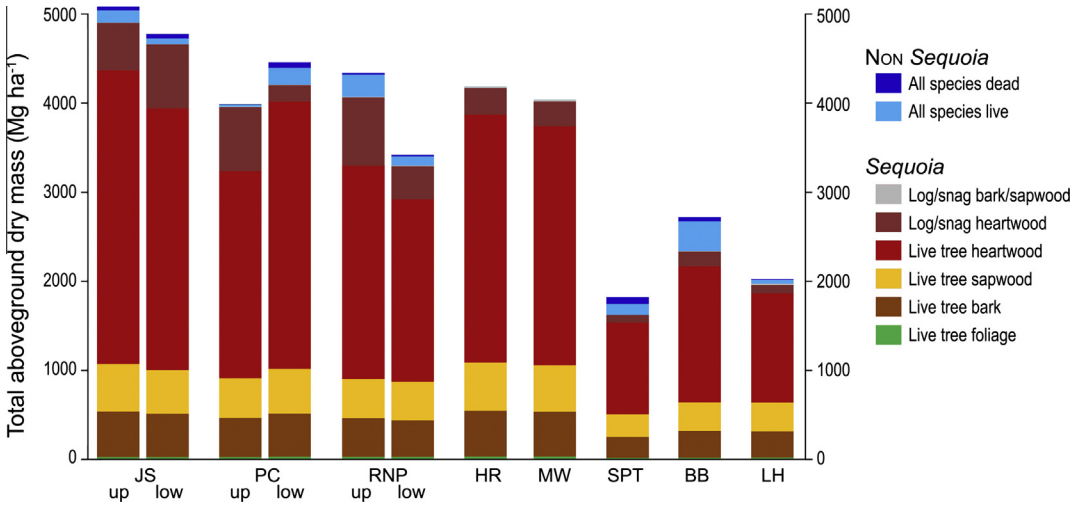

Fig. 9. Total aboveground mass summary. Two reddish colors represent heartwood of *Sequoia* from all live and dead trees, standing or fallen. Live tree heartwood includes dead wood within living trees. Note that *Sequoia* bark alone outweighs all other species combined in all but one plot. Forest floor horizons not quantified. (For interpretation of the references to color in this figure legend, the reader is referred to the web version of this article.)

ranging up to a single Codominant Canopy ensemble over 180 m long (HR). From the RH–CHM (which was scaled by trees >100 m tall in 7 of the 11 plots), the emergent nature of tree crowns was apparent, where spaces between trees often extended to the ground (Fig. 11). Unclassified sections were either unique or transitional between ensembles. A total of 15 Canopy Gap ensembles, occupying 285 m of centerline distance were large enough to be detected in eight plots and naturally had the lowest *Sequoia* LAI (1.2) and lowest total LAI (5.6) among ensembles (Table 8). The Canopy Gap ensemble had the highest deciduous LAI (0.6), containing the highest proportion of shade-intolerant species (Fig. 12).

Shared Dominance had a modest *Sequoia* LAI (4.7) but high contributions from other trees – *Notholithocarpus*, *Pseudotsuga*, and *Tsuga* (mean LAI = 6.0). Other non-*Sequoia* LAI was notable, including *Ericaceae* (0.8) and ferns (0.6). Total non-*Sequoia* LAI was 7.9, the highest of any ensemble (Fig. 12).

The three *Sequoia*-dominated ensembles were similar in that all had very high *Sequoia* LAI (mean 12.4), but they differed greatly in the sizes of contributing trees (Fig. 12). Apart from the size of trees contributing to the total, leaf areas between Emerging and Codominant Canopy ensembles were quite similar. In both cases, dense aggregations of *Sequoia* crowns kept non-*Sequoia* LAI to a minimum (mean 2.23), which was lower than the other ensembles. Of this, >90% consisted of the very shade-tolerant *Oxalis* and *Polystichum*.

Emergent Crowns had the highest total, highest *Sequoia*, and second highest non-*Sequoia* LAI as well as the highest contribution from large *Sequoia* (Table 8, Fig. 12). Emergent *Sequoia* crowns held enormous leaf areas, and most of the *Sequoia* LAI total came from trees >100 Mg. Simultaneously, 22% of the ensemble included RH-CHM values from the bottom three 5 m vertical tiers, which included a substantial non-*Sequoia* leaf area (LAI = 4.1) and the second highest deciduous LAI (0.2).

4. Discussion

We identified global maximum live biomass, leaf area, and total aboveground carbon by intensively measuring tall *Sequoia* forests across the range of the species in California. Our approach involved detailed plot work, hierarchical measurements, and stratified random sampling to generate equations for each species spanning the full size range of individuals in these forests. Spatially explicit application of allometric equations to quantify within-plot distributions of biomass and leaf area allowed us to perform structural analyses yielding strong support for light-use-complementarity (LUC – Ishii et al., 2013) in *Sequoia* forests with a basis in crown optimization and emergent facilitation.

4.1. Does emergent facilitation lead to LUC in Sequoia forests?

At the plot level, LUC is detectable using the Emergent Crown Index (ECI) and even more strongly by an analysis of structural ensembles. These findings coalesce around an ecological phenomenon whereby without stand-replacing disturbance, live biomass, leaf area, and aboveground carbon increase asymptotically over time through the development of emergent trees with deep crowns. Maxima in old-growth *Sequoia* forests occur in the oldest and most complex forests – a concept divergent from forest development models characterized by a peak and eventual decline of these variables over time (Coomes et al., 2012; Xu et al., 2012; Foster et al., 2014).

The highest values ever recorded for biomass (5190 Mg ha^{-1}), leaf area (LAI = 19.4), and aboveground carbon (2600 Mg ha^{-1}) occur in the same forest. This plot (JS-up) exemplifies emergent facilitation better than any other, as the Emergent Crowns ensemble occupies over half of the centerline length. Interestingly, this plot is in the only ocean-facing drainage within the wettest location throughout the range of *Sequoia*. While live *Sequoia* biomass is only slightly higher than that found in several other plots, large contributions to leaf area from other species (LAI = 8.0) are possible because of the organization of biomass into emergent trees. The additional leaf area from other species is equivalent to or exceeds the maximum in many of the world's forests (Asner et al., 2003), yet it occurs beneath the heaviest canopy on Earth.

Our results highlight important contributions of large trees to forest structure. Hinting at a possible universal pattern of forest structure, total biomass of Central African forests is well predicted by considering only the largest 5% of the trees (Bastin et al., 2015). Using only the largest trees is a novel approach to estimate the historically difficult metric of biomass. This method relates to emergent facilitation because the largest trees not only have the most mass, but also their spatial distribution provides the most information about how much light can penetrate the forest. Applying the Bastin et al. (2015) approach to tall *Sequoia* forests produces

Table 6
Carbon content of forest components in metric tons per hectare, highlighting the decay-resistant bark and heartwood of *Sequoia* (1 metric ton = 1 Mg = 1000 kg). Data do not include carbon from the forest floor or soil carbon. Note that 7 of the 11 plots have total C values ⩾2000 Mg ha^{-1}, and of that at least 1500 Mg ha^{-1} is *Sequoia* heartwood. Values in red are global maxima.

	Sequoia sempervirens only									All other species		
CARBON (Mg ha^{-1})	Leaf	Bark	Sapwood	Heartwood	Dead in live trees	Dead heartwood (snags and logs)	Total dead wood (snags and logs)	Total *Sequoia* heartwood	Live	Dead wood (snags and logs)	**Total Aboveground Carbon**
JS-up	10.0 ± 1.1	247 ± 15	260 ± 15	**1703 ± 60**	19.1 ± 1.8	265 ± 11	268 ± 11	**1968 ± 26**	68.2 ± 5.3	20.7 ± 0.7	**2596 ± 114**
JS-low	10.3 ± 1.0	236 ± 13	243 ± 13	1533 ± 51	13.7 ± 1.3	360 ± 16	361 ± 16	1893 ± 29	34.1 ± 4.2	25.6 ± 0.9	2456 ± 106
PC-up	9.8 ± 1.0	222 ± 13	231 ± 12	1264 ± 45	8.2 ± 0.9	363 ± 16	365 ± 16	1627 ± 28	14.0 ± 1.1	1.6 ± 0.1	2115 ± 97
PC-low	11.4 ± 1.1	234 ± 14	245 ± 11	1550 ± 41	17.4 ± 1.4	92 ± 5	94 ± 5	1642 ± 16	95.4 ± 3.2	30.8 ± 1.0	2278 ± 82
RNP-up	11.0 ± 1.1	209 ± 11	219 ± 11	1239 ± 42	9.7 ± 0.9	384 ± 15	386 ± 15	1623 ± 26	123.6 ± 9.0	10.0 ± 0.6	2207 ± 95
RNP-low	10.6 ± 1.1	199 ± 11	217 ± 11	1072 ± 36	6.3 ± 0.7	185 ± 8	189 ± 8	1258 ± 19	52.3 ± 3.4	9.7 ± 0.3	1755 ± 75
HR	12.7 ± 1.3	**253 ± 15**	275 ± 14	1479 ± 50	9.8 ± 1.0	151 ± 6	158 ± 7	1630 ± 21	0.4 ± 0.0	0.0 ± 0.0	2189 ± 95
MW	12.3 ± 1.2	244 ± 13	259 ± 14	1393 ± 46	11.0 ± 1.0	139 ± 5	149 ± 6	1532 ± 19	0.4 ± 0.0	0.0 ± 0.0	2069 ± 85
SPT	6.6 ± 0.7	119 ± 7	133 ± 7	567 ± 21	2.2 ± 0.3	43 ± 2	44 ± 2	610 ± 9	61.3 ± 2.1	38.2 ± 1.4	971 ± 46
BB	7.3 ± 0.8	144 ± 8	159 ± 9	793 ± 29	4.5 ± 0.5	83 ± 3	86 ± 3	876 ± 12	161.6 ± 6.6	24.0 ± 0.9	1380 ± 60
LH	8.3 ± 0.9	142 ± 8	163 ± 9	647 ± 24	1.4 ± 0.2	47 ± 2	53 ± 2	694 ± 11	21.4 ± 0.9	5.5 ± 0.1	1043 ± 48

markedly accurate results. For example, basal area of the 20 largest trees in each plot explains 92% of the variation in total live biomass and 69% of the variation in understory leaf area.

Crown optimization allows *Sequoia* to undergo a developmental trajectory whereby phenotypic plasticity of leaf form, foliage aggregation at multiple scales, and regrowth of damaged crowns operate together to maximize leaf area within individual crowns (Monsi and Saeki, 1953; Ishii and Asano, 2010, and Ishii et al., 2013). Other high leaf area forests are tall, conifer-dominated, and include trees with deep crowns (Leverenz and Hinckley, 1990). Because *Sequoia* is the tallest species and possesses decay-resistant heartwood, there are abundant opportunities for many trees to become emergent. The emergent trees we crown-mapped are >1100 years old and have complex crowns indicating previous damage and regrowth (Fig. 2). The largest and oldest of these trees are also among the fastest growing (Sillett et al., 2015a). Provided an individual *Sequoia* survives the ravages of fire and storms, development of an emergent tree may be inevitable.

When *Sequoia* trees first reach the upper canopy, they are still relatively young – 90 m trees can be completely model-conforming and without complex structure (Sillett and Van Pelt, 2007). They can then persist for millennia, not only repairing crown damage but also growing far larger. Within the classification of the eco-unit (Oldeman, 1990), a new structural ensemble appears – one where trees of the present have grown beyond to become emergent crowns of the future. During the long and variable process of becoming emergent, *Sequoia* trees often differ greatly in age from neighboring emergent trees. However, collectively they form a *structural cohort* known as the Emergent Crowns ensemble, containing the largest trees in the forest, which may or may not retain the original eco-unit boundary.

Identifying structural ensembles in *Sequoia* forests improves our ability to detect LUC beyond the plot-level metric of ECI. In this investigation, moving windows scaled to include trees adjacent to an emergent *Sequoia* define the minimum ensemble size. Depending on forest structure and species composition, ensembles can be large and persistent in old-growth forests (Fig. 11), and in younger forests such as plantations can be quite extensive (Oldeman, 1990). We suggest that moving window analyses in other forests use a search radius scaled by tree species and structural complexity to detect ensembles. Because *Sequoia* forests are so tall, it was relatively easy for us to detect the uppermost structural ensembles using LiDAR and to define five structural ensembles. In other forests, fewer ensembles may be detectable remotely, depending on the complexity of forest structure and resolution of the LiDAR point cloud.

Based on our experience in other tall forests that have emergent trees (*P. sitchensis*, *P. menziesii*, *S. giganteum*, and *Eucalyptus regnans*), detecting emergent trees using 0.75 h_{max} of the LiDAR canopy height model should also work well, since these forests can all develop similar old-growth structure (Franklin and Van Pelt, 2007). In shorter old-growth forests, emergent trees may be absent or if present may be wider, but only slightly taller, than neighboring trees (e.g., Amazonian rainforests, Appalachian Mountain cove forests), and a different h_{max} value may be more useful.

Just as an emergent *Sequoia* represents a developmental maximum at the scale of the tree, the Emergent Crowns ensemble represents a developmental maximum at the scale of the forest. Small-scale disturbances reset structure to Canopy Gap or Emerging Canopy ensembles, but natural developmental patterns inevitably guide structure toward one dominated by emergent trees (Fig. 13). Larger disturbances such as wildfire and wind throw revert forests to an earlier developmental stage, while smaller disturbances work to maintain the structural ensembles defined here. The *Sequoia* silvatic mosaic is a slowly shifting assemblage of eco-units, defined by relatively small-scales disturbances and

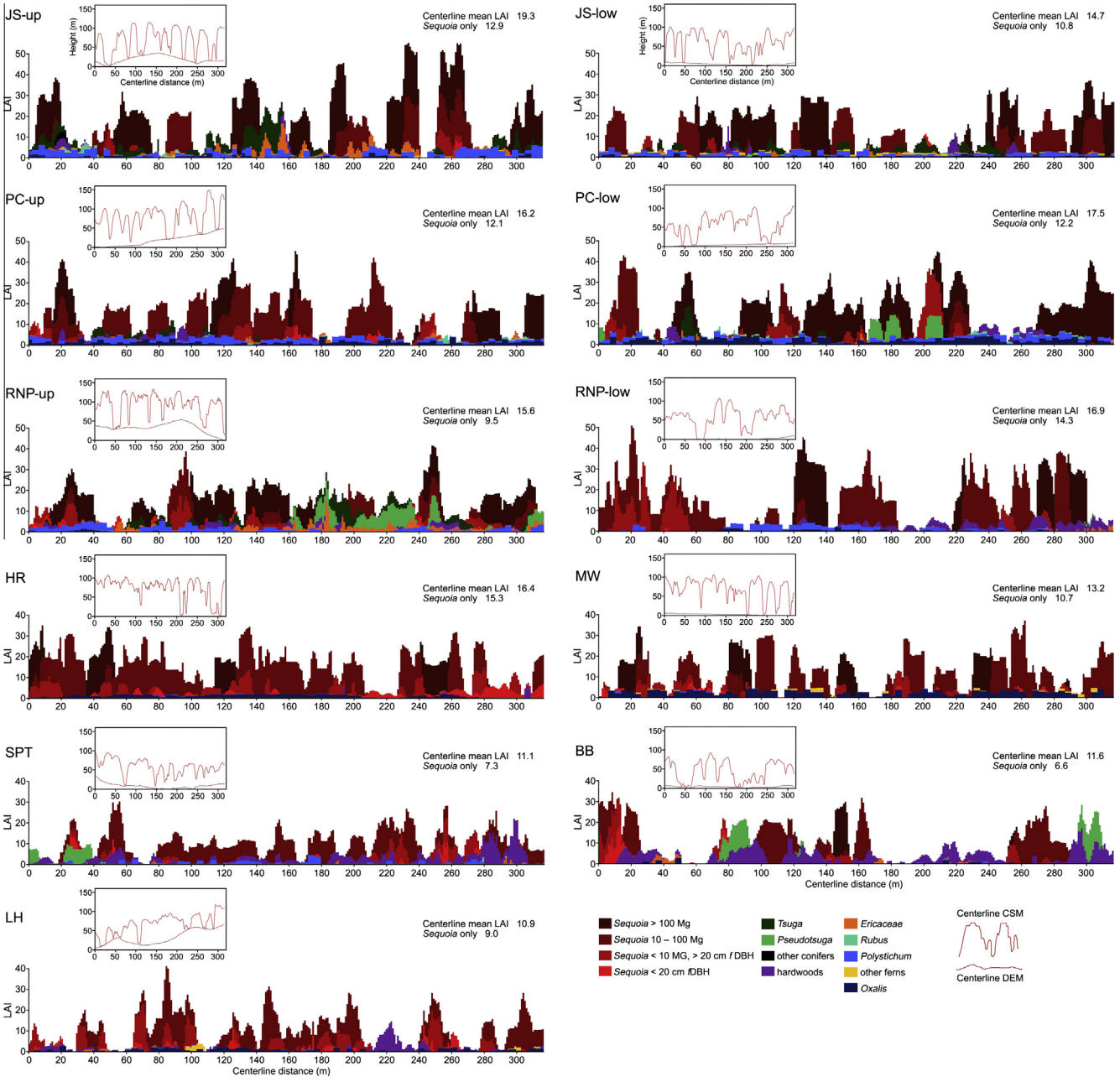

Fig. 10. Horizontal distribution of LAI. All plant crowns had leaf area partitioned into 1-m^2 cylinders along plot centerlines. LiDAR-derived CSM and DEM values (red and brown lines in inset graph) depict outer canopy and ground surface directly above centerline. Note that individual trees or tree clusters can have LAI > 30. Crowns of emergent trees evident in most plots as high leaf area values flanked by gaps. Note contributions from *Tsuga* and *Pseudotsuga* at RNP-up with their dominance occurring where plot passes over knoll (inset). (For interpretation of the references to color in this figure legend, the reader is referred to the web version of this article.)

regrowth over millennia. As these forests develop, crown optimization ensures progression toward the Emergent Crowns ensemble, which dominates six of our eleven plots. Codominant Canopy is the next most abundant ensemble and is not reflective of a disturbance (Canopy Gap) or recovery state (Emerging Canopy). Many Codominant Canopy ensembles have trees >1000 years old indicating that this ensemble not only takes centuries to form, but it also takes centuries for gap formation and subsequent crown optimization to progress toward the Emergent Crowns ensemble.

Within the old-growth *Sequoia* silvatic mosaic, the two most common single-tree or small group mortality events are burning in a fire or toppling from wind (Fig. 13). Even within rainforest portions of the range, fire is an important component of *Sequoia* forests, as large trees nearly always have charcoal on their bark, often visible well up into the crown of the tree (Brown and Swetnam, 1994; Sillett et al., 2015a). While it is unusual to see large individuals killed by fire, burn cavities at the bases of large trees are frequent in northern rainforests and nearly ubiquitous in drier southern forests. If trees are not killed, abundant sprouts (i.e., reiterated trunks) often emerge around tree bases after fire (Jameson and Robards, 2007). Multiple fires create different cohorts of sprouts, which can ultimately lead to development of *tree castles* – circular formations of successively larger stems leading into the central and largest trunk (Fig. 13). In such cases, charcoal is often present on the bark of all but the youngest cohort. Our southernmost plot (LH) is in a mixture of forest and chaparral, where fire is frequent. The most recent fires in this forest (1977,

Table 7
Emergent Crown Index (ECI). Seven structural metrics, all derived from either plot inventory, centerline analysis, or analysis of the LiDAR canopy height model. Values in bold represent the index maximum, and those in italics the 2nd highest. All R^2 have *P*-values <0.017.

Plot	Site	Plot level metrics				Individual tree metrics					Centerline variation		LiDAR detection – crowns at 0.75 h_{max} CHM						ECI
		Crown mass (kg)		Crown volume (m^3)		Median tree at 1/2 LAI		# trees to reach 1/2 LAI			Along centerline		Thiessen polygon distances (m)		Emergent crown size (m^2)				Mean of all 7 indices
		Mean	Index 1	SD	Index 2	Crown mass	Index 3	# trees	Scaled	Index 4	SD *Sequoia* LAI	Index 5	Mean	Index 6	Total area	Mean crown area	Count	Index 7	
JS-up	1	**5350**	**1.00**	4205	0.74	**10,191**	**1.00**	*14.0*	*1.17*	*0.86*	**13.88**	**1.00**	21.26	0.91	2647	71.5	37	0.77	*0.90*
JS-low	2	3304	0.62	3586	0.63	5661	0.56	16.3	1.36	0.74	9.59	0.69	20.99	0.90	2211	59.8	37	0.64	0.68
PC-up	3	1468	0.27	3217	0.56	2919	0.29	19.2	1.60	0.63	10.38	0.75	18.77	0.80	1962	49.0	40	0.53	0.55
PC-low	4	*4791*	*0.90*	**5713**	**1.00**	*10,099*	*0.99*	**12.0**	**1.00**	**1.00**	10.53	0.76	*22.36*	*0.95*	**2414**	**92.8**	**26**	**1.00**	**0.94**
RNP-up	5	2369	0.44	*4722*	*0.83*	5067	0.50	16.7	1.39	0.72	8.21	0.59	**23.43**	**1.00**	*1838*	*73.5*	*25*	*0.79*	0.70
RNP-low	6	891	0.17	2622	0.46	1496	0.15	24.0	2.00	0.50	*12.15*	*0.87*	20.40	0.87	1171	45.0	26	0.49	0.50
HR	7	1154	0.22	3016	0.53	2839	0.28	24.5	2.05	0.49	8.10	0.58	16.83	0.72	4653	51.7	90	0.56	0.48
MW	8	888	0.17	2559	0.45	2367	0.23	25.4	2.12	0.47	8.93	0.64	17.57	0.75	4022	43.7	92	0.47	0.45
SPT	9	862	0.16	2318	0.41	1252	0.12	22.4	1.87	0.53	5.82	0.42	17.95	0.77	1561	26.9	58	0.29	0.39
BB	10	857	0.16	2585	0.45	1742	0.17	18.3	1.53	0.66	9.39	0.68	19.82	0.85	1833	38.2	48	0.41	0.48
LH	11	263	0.05	1388	0.24	364	0.04	37.8	3.15	0.32	8.41	0.61	13.88	0.59	2003	40.1	50	0.43	0.33
R^2 with non-*Sequoia* LAI			0.69		0.53		0.64			0.67		0.49		0.63				0.51	0.74

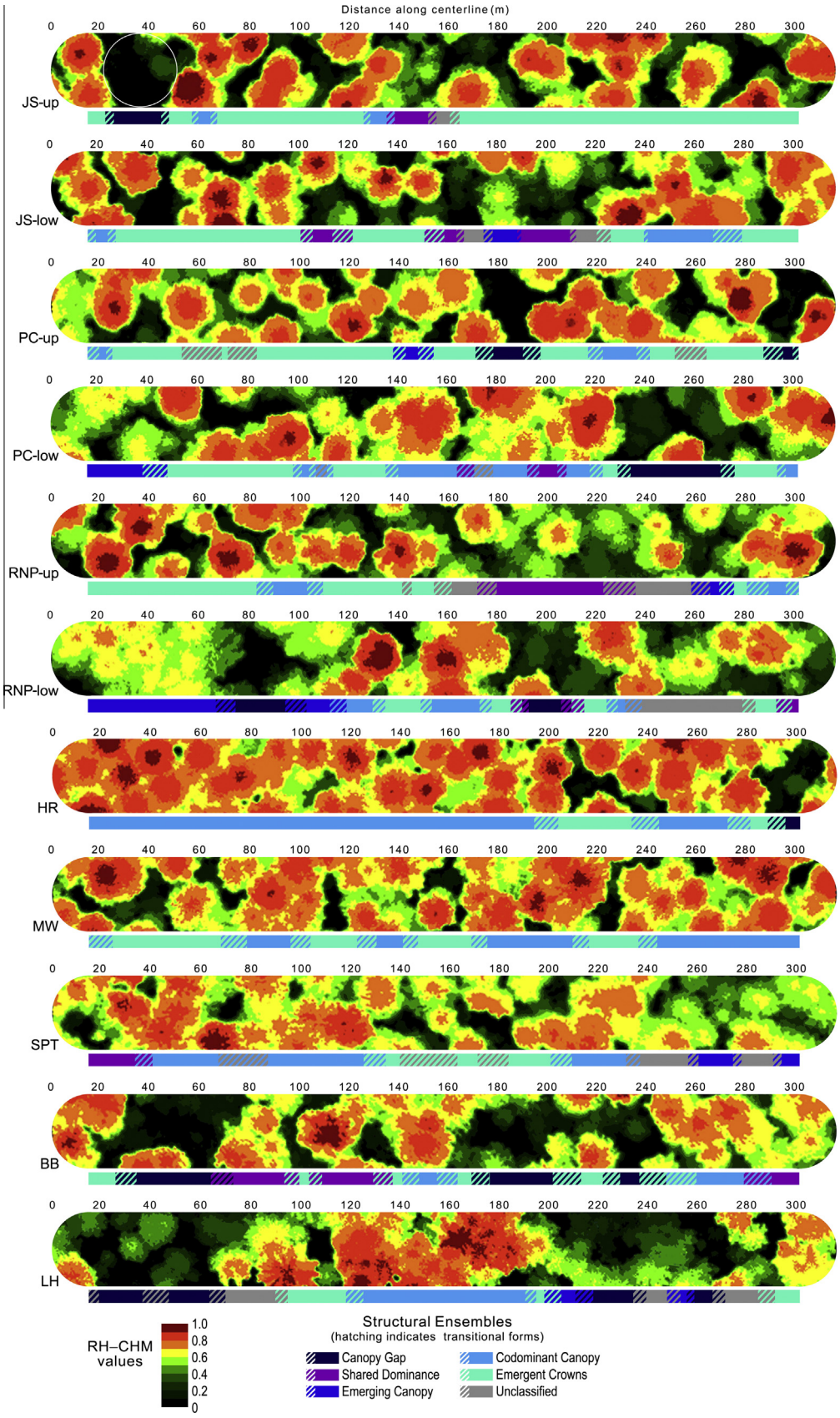

Fig. 11. RH–CHM maps for 11 plots. Analysis consisted of sampling 30-m-diameter moving window (white ring in upper left). Colored strip below each represents meter-by-meter classification of structural ensembles. The 15% unclassified ensembles (gray) were unique structurally or transitional between neighboring ensembles. (For interpretation of the references to color in this figure legend, the reader is referred to the web version of this article.)

Table 8
LAI breakdown by structural ensemble. Note than even though the **Emergent Crowns** ensemble had the highest *Sequoia* LAI, its non-*Sequoia* LAI was nearly as high as the **Canopy Gap** ensemble, despite having eight times more *Sequoia* foliage above. Total values not statistically different from each other have the same letter next to them.

		Canopy gap		Shared dominance		Emerging canopy		Codominant canopy		Emergent crowns	
Sequoia	>100 Mg	0.15 ± 0.09		2.39 ± 0.49		0.00 ± 0.00		2.52 ± 0.67		7.08 ± 0.38	
	10–100 Mg	0.41 ± 0.21		1.37 ± 0.24		9.00 ± 1.04		8.15 ± 0.70		5.34 ± 0.36	
	<10 Mg	0.64 ± 0.54		1.81 ± 0.59		2.37 ± 1.20		0.98 ± 0.16		1.13 ± 0.11	
	<20 cm	0.54 ± 0.48		0.24 ± 0.06		0.08 ± 0.05		0.38 ± 0.09		0.20 ± 0.04	
	Sequoia total	1.74 ± 1.32	a	4.81 ± 1.37	a	11.45 ± 2.29	b	12.04 ± 1.62	b	13.75 ± 0.89	b
	Pinaceae	0.49 ± 0.55		4.98 ± 0.59		0.12 ± 0.20		0.00 ± 0.02		0.96 ± 0.38	
	Deciduous	0.59 ± 0.12		0.02 ± 0.12		0.12 ± 0.21		0.03 ± 0.15		0.22 ± 0.08	
	Evergreen	2.76 ± 0.10		2.94 ± 0.08		2.12 ± 0.92		2.07 ± 0.78		2.93 ± 0.06	
	Non-*Sequoia* total	3.84 ± 0.77	c	7.94 ± 0.79	d	2.36 ± 1.33	c	2.10 ± 0.94	c	4.11 ± 0.52	c
	Total LAI	5.58 ± 2.09	e	12.75 ± 2.16	f	13.81 ± 3.62	fg	14.14 ± 2.56	fg	17.86 ± 1.41	g

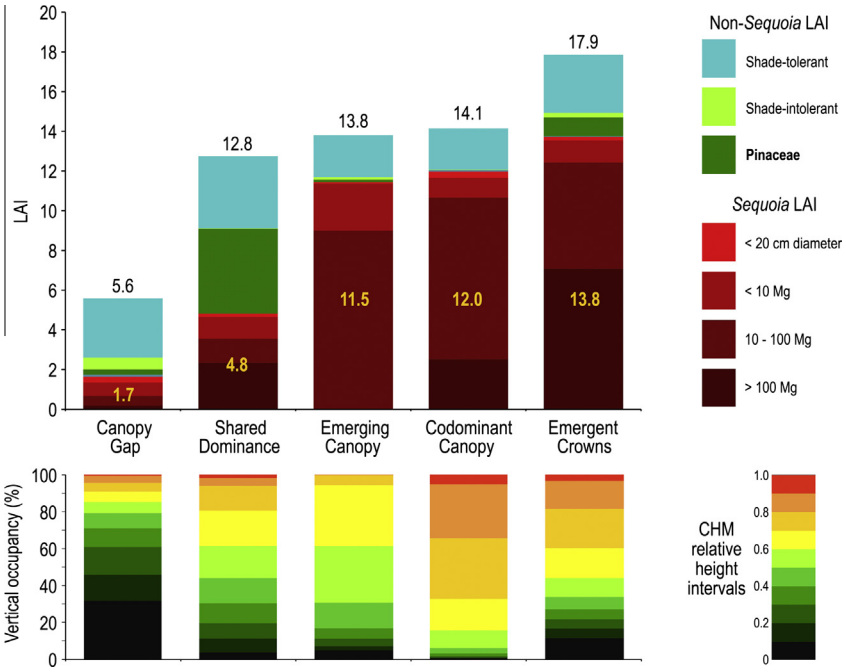

Fig. 12. Leaf area within structural ensembles. Values are means from all sites combined – black values above bars are all species LAI, and yellow values within bars are *Sequoia* only. Top panel shows Emergent Crowns had highest *Sequoia* LAI while simultaneously having relatively high LAI in all three non-*Sequoia* categories. Note that more than half of *Sequoia* LAI in Emergent Crowns came from trees >100 Mg. Bottom panel shows mean RH–CHM values for each ensemble. Note that Emergent Crowns was the only ensemble to have >3.5% represented in all ten height bands. (For interpretation of the references to color in this figure legend, the reader is referred to the web version of this article.)

1985, 1999, 2008) all started by lightning (Rowntree, 2009). In general, the hottest portions of these burns exhibit severe fire effects on the vegetation including mortality of *Sequoia*. However, like most of the chaparral plants sympatric with *Sequoia* in this area, sprouting from lignotubers at the base usually follows death of aboveground parts (Hanes, 1971; Farjon, 2005). Genetic individuals may persist below ground, but frequent fire limits longevity, making trees >1000 years extremely rare in southern *Sequoia* forests.

The most common way large *Sequoia* die is through toppling (Fig. 13). Winter is the wettest and windiest time of year and brings normal winter storms as well as periodic atmospheric rivers. The latter originate from tropical cyclones and bring tremendous amounts of rain and high winds over a short time and are responsible for the most extreme events along the west coast of North America (Waring and Franklin, 1979; Henderson et al., 1989; Zhu and Newell, 1998; Ralph et al., 2004). With tall trees commonly carrying 100–200 Mg of biomass or more, high winds combined with saturated soils can cause tilting of trees. For trees that become as tall, large, and old as *Sequoia*, even a slight lean only gets worse. Partial crown damage as well as snapping of the upper stem occur during such events, but large *Sequoia* trees that topple from their base expose roots and mineral soil. Toppling of large trees is uncommon but is nearly always predisposed by lean (R. Van Pelt and S. C. Sillett, *personal observations*). Root decay is often a precursor to toppling with many Pacific Northwest tree species (Spies et al., 1990; Bible, 2001; Franklin et al., 2002; Van Pelt, 2007) but much less so with *Sequoia*, so when whole trees fall there is usually a large root-plate still intact (Boe, 1966 – Fig. 6 shows several >5 m wide).

The Shared Dominance ensemble is highly variable, especially in regards to emergent facilitation. In rainforest plots, most of the non-*Sequoia* contribution is *Tsuga*, which establishes on logs from seed and readily grows in the penumbra beneath tall canopies, much as it does in old-growth forests throughout the Pacific Northwest. In cases where it is abundant enough to define a Shared

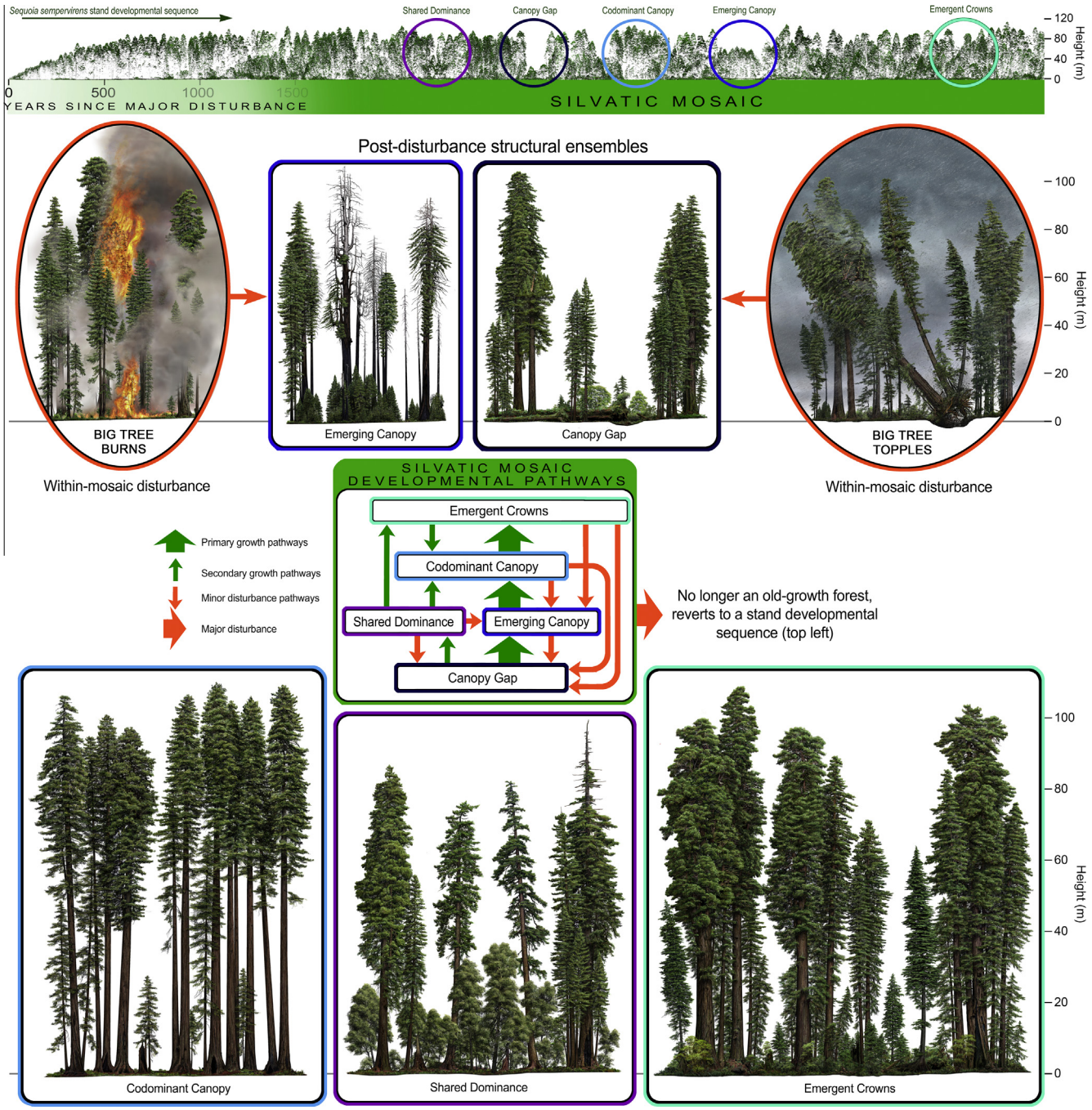

Fig. 13. Flowchart depicting transitions between structural ensembles in old-growth *Sequoia* forests. Green arrows indicate a natural growth trajectory, and orange arrows indicate disturbances that reset ensembles. Orange ellipses represent two most common disturbance events that alter ensembles, and arrows from them indicate possible outcomes. Emerging Canopy is probably the most variable structural ensemble – the result of many possible disturbance/recovery scenarios. Larger disturbances that reset the forest into a stand development pathway (see timeline, far upper left) are not shown. Tree castles are visible on far right of both Emergent Crowns and Shared Dominance profiles. (For interpretation of the references to color in this figure legend, the reader is referred to the web version of this article.)

Dominance ensemble, the forest is in a transitional state where replacement of dead *Sequoia* by younger *Sequoia* is slow. In the southern plots, most of the Shared Dominance ensembles are associated with *Pseudotsuga* and *Notholithocarpus*. Both species do well after fire by either reseeding or basal sprouting, respectively, so are common associates of *Sequoia* in drier forests. Both can be locally dominant in small patches, but in many cases the eco-unit will eventually return to a *Sequoia*-dominated ensemble by virtue of its reiterative capacity, shade tolerance, and longevity. Despite each plot being located in a tall, old-growth forest, along the 316 m length there are naturally edaphic conditions where *Sequoia*-dominance may never be realized, including knolls and steep slopes where other species will probably always be significant contributors. These areas become much more abundant in the greater silvatic mosaic, so structural ensemble criteria would be altered to address shorter canopies of forests on upper slopes and ridges, even within *Sequoia*-dominated landscapes.

4.2. Are emergent trees essential to achieving maximum leaf area?

Sequoia forests eventually reach a stage of structural development where very high leaf area is maintained in perpetuity, an idea

that has long been debated (Fritz, 1932; Roy, 1966). Our findings are contrary to widely accepted models of forest development that suggest leaf area peaks shortly after canopy closure and then slowly declines (Gower et al., 1996; Ryan et al., 1997; Binkley et al., 2002) or quickly reaches a peak and remains relatively constant thereafter (Turner and Long, 1975; Long and Smith, 1992). However, we acknowledge that leaf area is extremely difficult to quantify accurately at the plot level, no matter what techniques are used – especially in tall conifer forests (Chen and Cihlar, 1995; Bréda, 2003).

Maximum canopy occupancy occurs during the canopy closure phase of forest development, because afterwards small-scale gaps from fallen and dead trees, as well as tree-to-tree abrasion, allow light to penetrate between crowns (Putz et al., 1984; Long and Smith, 1992; Franklin et al., 2002). Consequently, maximum canopy occupancy has often been identified by a lack of understory and used to indicate that all available light is being used by overstory tree species and that a forest has attained maximum leaf area. Moving from a two-dimensional view to three dimensions, and considering penumbral effects and crown optimization, taller forests are always able to support more leaves than shorter ones (Kira and Shidei, 1967; Horn, 1971; Waring, 1983). In many instances differences in leaf area between forests with closed canopies and tall old-growth forests are small – frequently smaller than the error bars surrounding plot-level leaf area estimates. For example, a fully-stocked 21-year-old *Sequoia* plantation on the same floodplain as our HR plot (*Sequoia* LAI = 14.5) has nearly identical leaf area (LAI = 14.3 – O'Hara et al., 2007). In the plantation, canopy occupancy is at a maximum suggesting that leaf area is probably near the upper limit for *Sequoia*. *Sequoia* plantations have such dense canopies that full shade (umbra) reaches the ground and thus not enough light remains to support an understory. The HR plot, which is dominated by the Codominant Canopy ensemble, has a remarkable 37 TPH > 90 m tall, leaving only 11.2% open space at 70 m above the ground. This plot has the lowest understory leaf area among our eleven plots, but in contrast to the plantation enough penumbral light is available near ground level to support an understory LAI of 1.8, some of which is *Sequoia* regeneration (LAI = 0.6). Thus, both forests have extremely high *Sequoia* leaf area, but the taller forest has higher light availability at ground level, providing an increase in both species diversity and total leaf area. By building emergent trees, *Sequoia* leaf area remains high while light penetration through the canopy vastly increases.

Rainforest plots have by far the most massive understories and none more than the three plots in drainages exposed to the ocean (JS-up, PC-up, and PC-low). These plots have consistently higher understory leaf areas (mean LAI = 4.9) than the three rainforest plots sheltered behind ridges (mean LAI = 2.6). While we do not have detailed data on cloud or fog cover for our plots, ocean-facing drainages tend to have less annual sunshine than those behind ridges as a consequence of coastal fog in California (Filonczuk et al., 1995; O'Brien et al., 2013; USGS, 2015). In cloudy environments, the umbra behind an object is diminished, allowing leaf layers to be closer than in sunny environments (Horn, 1971). Understories of *Sequoia* rainforests are compositionally similar with dominance switching between *V. ovatum* and *P. munitum* (and to a lesser extent *B. spicant*) – *Vaccinium* growing on accumulated rotten wood and ferns growing elsewhere. *V. ovatum* has dense evergreen leaves, which are small (1–2 cm diameter), while fern fronds can be quite large (>2 m long). However, *Polystichum* and *Blechnum* fronds are divided into pinna at ~1-cm spacing, which collectively create a light environment similar to that beneath small leaves. In cloudy or foggy conditions, frond pinnae are ideally spaced to avoid creating an umbra for subtending pinnae. These three understory species efficiently capture penumbral light. A fourth species, the diminutive and shade-tolerant *Oxalis* is generally found under the shrubs and ferns to capture any remaining light. These four species are in large part responsible for the high non-*Sequoia* leaf area in rainforest plots, providing 82–95% of the understory total.

4.3. How do aboveground carbon and abundance of dead wood vary across old-growth Sequoia forests in California?

The eight northern plots have total aboveground carbon contents >2000 Mg ha^{-1}, which is nearly twice that reported for any other forest type (Franklin and Waring, 1980; Keith et al., 2014; Sillett et al., 2015b). What makes this situation even more extreme is that 63–77% of the carbon is embedded in decay-resistant *Sequoia* heartwood. Within the rainforest part of the range, the wet environment, coupled with the infrequency and patchiness of fires, allows heartwood to accumulate and persist for centuries. Fine woody debris and forest floor litter were not sampled in this study, but this material was sampled in nearby forests covering the area of our 7 northernmost plots (Graham, 2009) and contributes another 30–60 Mg ha^{-1} dry mass (Appendix P).

Maximum carbon sequestration occurs in forests combining exceptionally productivity (Waring and Franklin, 1979; Larjavaara and Muller-Landau, 2011) and carbon storage in dead wood (Harmon, 2001; Luyssaert et al., 2008). In dry or otherwise fire-prone areas where dead wood is consumed by fire, or where logs quickly decay between a combination of saturation under winter snowpack and desiccation during hot summers, nearly all aboveground carbon exists in live trees. Carbon storage in these forests depends on tree longevity, or time until the next major disturbance perturbs the tree population (Zhang et al., 2010; North and Hurteau, 2011). In wet forests, where saturated logs resist decay and infrequent fires often lack ability to combust large logs, dead wood represents a quarter to nearly half of aboveground carbon mass (Grier and Logan, 1977; Harmon et al., 2004). Like our rainforest plots with dead wood masses approaching 400 Mg ha^{-1} of carbon, nearly all other dead wood masses >250 Mg ha^{-1} of carbon come from either temperate rainforests in the Pacific Northwest (Grier et al., 1981; Agee and Huff, 1987; Keenan et al., 1993; Smithwick et al., 2002) or Tasmania (Dean et al., 2003; Keith et al., 2009; Moroni et al., 2010). Another high value is from a 2290 Mg ha^{-1} *Agathis australis*–dominated rainforest in subtropical New Zealand, where 225 Mg ha^{-1} of carbon is dead wood (Silverster and Orchard, 1999).

Critical considerations for residence time of forest carbon are the amount, size, and composition of dead wood inputs as well as fire regime (Spies et al., 1988; Agee, 1993; Harmon, 2001). These factors explain the increasing ability of *Sequoia* forests to store carbon as one moves north along coastal California's precipitation gradient. Large-diameter logs of *P. menziesii* commonly persist for at least two centuries in old-growth rainforests (Sollins et al., 1987; Spies et al., 1988) and sometimes for over four (Franklin et al., 1981). Radiocarbon dating reveals that *T. plicata* can persist as logs for at least 1300 years due to decay-resistant heartwood (Daniels et al., 1997). Like *Thuja*, heartwood produced by other members of the *Cupressaceae* is decay-resistant (Clark and Scheffer, 1983; Farjon, 2005), and they produce persistent logs in their respective rainforests around the Pacific Rim (Andrews, 1985; Feller, 2003; Keith et al., 2009). Since *Sequoia* is not succeeded by other species and has the most decay-resistant wood in the region, the greatest accumulations of dead wood come from forests with the largest trees. These inputs take the form of large logs composed mostly of decay-resistant heartwood favoring long carbon residence time.

Carbon losses from forest ecosystems primarily come from decomposition and fire. Both sources of loss decrease from south to north along the California coast. Carbon gains related to productivity in temperate forests are controlled chiefly by precipitation

(Rosenzweig, 1968; Whittaker, 1970), leaf area (Gholz, 1982), and live biomass (Keeling and Phillips, 2007), all of which increase from south to north along the California coast. Thus, persistence of dead wood, amount of live wood, and maximum carbon storage are all highest in *Sequoia* rainforests.

4.4. Comparisons with other forests

If the largest species in a forest is also a shade-intolerant pioneer, biomass increases during stand development to a maximum and then declines. These forests cannot maintain record biomass over long periods. Such is the case with tall *P. menziesii* forests in the Pacific Northwest and *E. regnans* forests in southeast Australia, which share many of aspects of emergent facilitation with *Sequoia*. In both forest types, the dominant trees are attacked by fungal decay more readily than *Sequoia*, and their relative shade intolerance limits future recruitment in the absence of mid- to large-scale disturbances. Thus, both species form nearly pure stands after high-severity fires, grow quickly, often do not regenerate without further disturbances, are dominant for centuries, and contribute to some of the highest non-*Sequoia* forest biomasses known (Van Pelt et al., 2004; Sillett et al., 2015b). In low-elevation rainforests of the Pacific Northwest, *Pseudotsuga* can maintain dominance for >500 years, by which time the few remaining individuals become emergent trees with enormous crowns (Van Pelt and Sillett, 2008) and plot-level biomass and leaf area reach a maximum (Franklin and Van Pelt, 2004). After 4–7 centuries, however, fungal decay is rampant (Franklin et al., 2002; Van Pelt, 2007) and without further disturbances to allow regeneration, emergent *Pseudotsuga* begin to collapse, which causes permanent reductions in canopy height, biomass, leaf area, and structural complexity as they are replaced by smaller, shade-tolerant species (Turner and Long, 1975; Franklin et al., 2002; Van Pelt and Nadkarni, 2004). A very similar scenario can be drawn for *E. regnans*, where without secondary disturbances, emergent trees eventually succumb to decay and are replaced by smaller shade-tolerant species with concurrent reductions in forest-level biomass and leaf area (Ashton, 2000; Wood et al., 2010; Tng et al., 2014).

In contrast, biomass of some forests may increase asymptotically toward a theoretical maximum. Primary forests in the wet tropics have continuous forest cover spanning generations of trees, such that the oldest living dominants established under forest conditions (Leigh et al., 1982; Brokaw, 1985; Oldeman, 1990; Clark and Clark, 1992). Developmentally similar temperate forests are dominated by *Cupressaceae* in wet coastal mountains around the Pacific Rim. *Chamaecyparis*, *Cryptomeria*, *Cupressus*, *Fitzroya*, *Sequoia*, *Taiwania*, and *Thuja* can all live >1500 years (Carder, 1995; Van Pelt, 2001; Farjon, 2005, 2008; Earle, 2015; Sillett et al., 2015a). Even with trees so old, the forests in which they grow may be much older because shade-tolerant individuals attain canopy dominant positions in the absence of stand-replacing disturbances (Fritz, 1957; Veblen and Ashton, 1982; Kojo, 1987; Franklin et al., 1988; Enright and Hill, 1996; Farjon, 2005; Van Pelt, 2007; Lorimer et al., 2009). When the age of a forest is much greater than the age of its oldest trees, forest age becomes irrelevant, and biomass and leaf area may continue to accumulate over time.

Age-related declines in forest *productivity* are frequently reported (Bormann and Likens, 1979; Ryan et al., 1997), and since biomass increment is strongly related to leaf area (Sillett et al., 2015a,b; Koch et al., 2015), this implies declining leaf areas in old forests. Quantifying leaf area and productivity of forest plots is difficult, as the chronosequence approach often suffers from design considerations, and plot re-measurements often occur over relatively short intervals (Foster et al., 2014). Long-term research, however, has shown that this decline is not attributed to an age-related decline in tree-level productivity, but rather to changes in forest structure caused by mortality of large trees (Coomes et al., 2012; Xu et al., 2012). In these cases, limits on the longevity of individuals led to measured declines. In an example from northern Minnesota where tree rings were used to examine growth, an age-related decline was observed with an interesting exception. A low-productivity old-growth forest dominated by multi-cohort *Quercus rubra* containing a significant component of *Thuja occidentalis* (*Cupressaceae*) exhibited an essentially asymptotic increase in biomass increment over time (Foster et al., 2014). In cases where the largest species in the forest can regenerate under forest conditions, aboveground biomass and leaf area may approach a theoretical maximum.

4.5. Conclusions

This is the first study to quantify the magnitude of aboveground biomass, leaf area, and carbon in *Sequoia* forests across the range of the species, whose grandeur has long captivated society. Our results provide an explanation of how established *Sequoia* forests achieve dimensions far beyond those of any other forest in the world and can continue to approach a theoretical maximum in perpetuity. *Sequoia* forests excel at all of the key variables necessary for crown optimization – phenotypic plasticity of leaf form, tall structures on which to build emergent crowns, extremely decay-resistant heartwood, and prolific capacity for reiteration, which permit recovery from crown damage and promote longevity. In addition, since *Sequoia* is not succeeded by other species, maxima in biomass, leaf area, and aboveground carbon are essentially asymptotic over time. *Sequoia* is unmatched in both the amount and type of carbon stored in old-growth forests. Because >95% of the original *Sequoia* forests have been cut at least once, management of younger forests toward this goal will benefit from better predictions of biomass and leaf area. This study presents a *snapshot* of aboveground biomass, leaf area, and carbon in eleven plots based on a single, intensive field visit. We are also making five-year re-measurements of every variable, including ground-based subsampling and within-crown measurements, to quantify aboveground biomass increments and rates of carbon sequestration in these forests as well those dominated by *Sequoia*'s closest living relative, *Sequoiadendron*.

Acknowledgments

This research was supported by the Save the Redwoods League (Redwoods and Climate Change Initiative), the Kenneth L. Fisher Chair of Redwood Forest Ecology at Humboldt State University, and the National Science Foundation (IOB-0445277). We thank our primary crew Anthony Ambrose, Marie Antoine, Ethan Coonen, Giacomo Renzullo, Kalia Scarla, and Jim Campbell-Spickler, who were responsible for much of the climbing and branch dissections. We also thank Scott Altenhoff, Wakana Azuma, Wendy Baxter, Nolan Bowman, Emily Burns, Allyson Carroll, Todd Dawson, Ken Fisher, Hiroaki Ishii, Nick Kent, Bryan Kotwica, Dan Krauss, Rikke Reese Næsborg, Tobe Sherrill, Cameron Williams, Chris Wong, and the Forest Measurements and Silvics classes at Humboldt State University from 2011 to 2013. We are grateful to several California State Parks (Big Basin Redwoods, Humboldt Redwoods, Jedediah Smith Redwoods, Prairie Creek Redwoods, and Samuel P. Taylor), Montgomery Woods State Natural Reserve, Landels–Hill Big Creek Reserve, Redwood National Park, and the Arcata Community Forest for granting permission to establish long term plots, climb trees, collect samples within these reserves, and for help with logistics. Jerry Franklin provided valuable input on the structure of the paper.

Appendix A. Supplementary material

Supplementary data associated with this article can be found, in the online version, at http://dx.doi.org/10.1016/j.foreco.2016.05.018.

References

Agee, J.K., 1993. Fire Ecology of Pacific Northwest Forests. Island Press, Washington, DC, 505 p.

Agee, J.K., Huff, M.H., 1987. Fuel succession in a western hemlock/Douglas-fir forest. Can. J. For. Res. 17, 697–704.

Alaback, P.B., 1986. Biomass regression equations for understory plants in coastal Alaska: effects of species and sampling design on estimates. Northwest Sci. 60, 90–103.

Alaback, P.B., 1991. Comparative ecology of temperate rainforests of the Americas along analogous climatic gradients. Rev. Chil. Hist. Nat. 64, 399–412.

Anderson, M.C., 1964. Studies of the woodland light climate. I. The photographic computation of light conditions. J. Ecol. 52, 27–41.

Andrews, R.W., 1985. Redwood Classic. Schiffer Publishing Limited, West Chester, PA, 174 p.

Ashton, D.H., 2000. The environment and plant ecology of the Hume Range, central Victoria. Proc. R. Soc. Victoria 112, 185–278.

Asner, G.P., Scurlock, J.M.O., Hicke, J.A., 2003. Global synthesis of leaf area index observations: implications for ecological and remote sensing studies. Glob. Ecol. Biogeogr. 12, 191–205.

Bastin, J.-F., Barbier, N., Réjou-Méchain, M., Fayolle, A., Gourlet-Fleury, S., Maniatis, D., de Haulleville, T., Baya, F., Beeckman, H., Beina, D., Couteron, P., Chuyong, G., Dauby, G., Doucet, J.-L., Droissart, V., Dufrêne, M., Ewango, C., Gillet, J.F., Gonmadje, C.H., Hart, T., Kavali, T., Kenfack, D., Libalah, M., Malhi, Y., Makana, J. R., Pélissier, R., Ploton, P., Serckx, A., Sonké, B., Stevart, T., Thomas, D.W., De Cannière, C., Bogaert, J., 2015. Seeing Central African forests through their largest trees. Sci. Rep. 5 (August 17) 13156.

Bible, K.J., 2001. Long-term Patterns of Douglas-fir and Western Hemlock Mortality in the Western Cascade Mountains of Washington and Oregon Ph.D. Dissertation. University of Washington, Seattle, WA, 85 p.

Binkley, D., Stape, J.L., Ryan, M.G., Barnard, H.R., Fownes, J., 2002. Age-related decline in forest ecosystem growth: an individual-tree, stand-structure hypothesis. Ecosystems 5, 58–67.

Boe, K.N., 1966. Windfall after experimental cuttings in old-growth redwood. Soc. Am. For. Proc. 1965, 59–62.

Bormann, F.H., Likens, G.E., 1979. Catastrophic disturbance and the steady-state in Northern hardwood forests. Am. Sci. 67, 660–669.

Bréda, N., 2003. Ground-based measurements of leaf area index: a review of methods, instruments and current controversies. J. Exp. Bot. 54, 2403–2417.

Brokaw, N.V.L., 1985. Gap-phase regeneration in a tropical forest. Ecology 66, 682–687.

Brown, J.K., 1974. Handbook for Inventorying Downed Woody Material. USDA Forest Service INT-GTR-16, Ogden, Utah, 24 p.

Brown, P.M., Swetnam, T.W., 1994. A cross-dated fire history from coast redwood near Redwood National Park, California. Can. J. For. Res. 24, 21–31.

Burrascano, S., Keeton, W.S., Sabatini, F.M., Blasi, C., 2013. Commonality and variability in the structural attributes of moist temperate old-growth forests: a global review. For. Ecol. Manage. 291, 458–479.

Canham, C.D., 1988. Growth and canopy architecture of shade-tolerant trees: response to canopy gaps. Ecology 69, 786–795.

Carder, A.C., 1995. Forest Giants of the World: Past and Present. Fitzhenry and Whiteside, Markham, Ontario, 208 p.

Carroll, A.L., Sillett, S.C., Kramer, R.D., 2014. Millennium-scale crossdating and inter-annual climate sensitivities of standing California redwoods. PLoS ONE 9, 1–18.

Chen, J.M., Cihlar, J., 1995. Quantifying the effect of canopy architecture on optical measurements of leaf area index using two gap size analysis methods. IEEE Trans. Geosci. Remote Sens. 33, 777–787.

Clark, D.A., Clark, D.B., 1992. Life history diversity of canopy and emergent trees in a neotropical rain forest. Ecol. Monogr. 62, 315–344.

Clark, J.W., Scheffer, T.C., 1983. Natural decay resistance of the heartwood of coast redwood *Sequoia sempervirens*. For. Prod. J. 33, 15–20.

Coomes, D.A., Holdaway, R.J., Kobe, R.K., Lines, E.R., Allen, R.B., 2012. A general integrative framework for modeling woody biomass production and carbon sequestration rates in forests. J. Ecol. 100, 42–64.

Daniels, L.D., Dobry, J., Klinka, K., Feller, M.C., 1997. Determining year of death of logs and snags of *Thuja plicata* in southwestern coastal British Columbia. Can. J. For. Res. 27, 1132–1141.

Dean, C., Roxburgh, S., Mackey, B.G., 2003. Growth modeling of Eucalyptus regnans for carbon accounting at the landscape scale. In: Amaro, A., Reed, D., Soares, P. (Eds.), Modeling Forest Systems. ACBI, Wallingford, UK, pp. 27–40.

Duncan, W., 1971. Leaf angles, leaf area, and canopy photosynthesis. Crop Sci. 11, 482–485.

Earle, C., 2015. Roster of the ancients. The Gymnosperm Database. <www.conifers.org/topics/oldest.htm>.

Enright, N.J., Hill, R.S. (Eds.), 1996. Ecology of the Southern Conifers. Smithsonian Institution Press, Washington, DC, 352 p.

Falster, D.D., Westoby, M., 2003. Leaf size and angle vary widely across species: what consequences for light interception? New Phytol. 158, 509–525.

Farjon, A., 2005. A Monograph of Cupressaceae and *Sciaopitys*. Royal Botanic Gardens, Kew.

Farjon, A., 2008. A Natural History of Conifers. Timber Press, Portland, 304 p.

Feller, M.C., 2003. Coarse woody debris in the old-growth forests of British Columbia. Environ. Rev. 11, 135–157.

Filonczuk, M.K., Cayan, D.R., Riddle, L.G., 1995. Variability of Marine Fog along the California Coast. Scripps Institution of Oceanography Report 95-2, 102 p.

Foster, J.R., D'Amato, A.W., Bradford, J.B., 2014. Looking for age-related growth decline in natural forests: unexpected biomass patterns from tree rings and simulated mortality. Oecologia 175, 363–374.

Franklin, J.F., Waring, R.H., 1980. Distinctive features of the northwestern coniferous forest: development, structure, and function. In: Waring, R.H. (Ed.), Forests: Fresh Perspectives from Ecosystem Analysis. Oregon State University Press, Corvallis, pp. 59–86.

Franklin, J.F., Cromack Jr., K., Denison, W., McKee, A., Maser, C., Sedell, J., Swanson, F., Juday, G., 1981. Ecological Characteristics of Old-Growth Douglas-Fir Forests. USDA Forest Service PNW-GTR-118, 48 p.

Franklin, J.F., Moir, W.H., Hemstrom, M.A., Greene, S.E., Smith, B.G., 1988. The forest communities of Mount Rainier National Park. Scientific Monograph Series No. 19. National Park Service, 194 p.

Franklin, J.F., Spies, T.A., Van Pelt, R., Carey, A.B., Thornburgh, D.A., Berg, D.R., Lindenmayer, D.B., Keeton, W.S., Shaw, D.C., Bible, K., Chen, J., 2002. Disturbances and structural development of natural forest ecosystems with silvicultural implications, using Douglas-fir forests as an example. For. Ecol. Manage. 155, 399–423.

Franklin, J.F., Van Pelt, R., 2004. Spatial aspects of complexity in old-growth forests. J. For. 102, 22–28.

Fritz, E., 1932. The Role of Fire in the Redwood Region. University of California Agricultural Experiment Station Circular 323.

Fritz, E., 1957. The life and habits of redwood the extraordinary. Western Conserv. J. 14, 4–7.

Fujimori, T., 1977. Stem biomass and structure of a mature *Sequoia sempervirens* stand on the Pacific coast of northern California. J. Jpn. For. Soc. 59, 435–441.

Gholz, H.L., 1982. Environmental limits on aboveground net primary production, leaf area, and biomass in vegetation zones of the Pacific Northwest. Ecology 63, 469–481.

Gower, S.T., McMurtrie, R.E., Murty, D., 1996. Aboveground net primary production decline with stand age: potential causes. Trends Ecol. Evol. Res. 11, 378–382.

Graham, B.B., 2009. Structure of downed Woody and Vegetative Debris in Old-Growth *Sequoia sempervirens* Forests MS Thesis. Humboldt State University, 101 p.

Grier, C.C., Logan, R.S., 1977. Old-growth *Pseudotsuga menziesii* communities of a western Oregon watershed: biomass distribution and production budgets. Ecol. Monogr. 47, 373–400.

Grier, C.C., Vogt, K.A., Keyes, M.R., Edmonds, R.L., 1981. Biomass distribution and above-and below-ground production in young and mature *Abies amabilis* zone ecosystems of the Washington Cascades. Can. J. For. Res. 11, 155–167.

Griffin, J.R., Critchfield, W.B., 1972. The Distribution of Forest Trees in California. USDA Forest Service PSW-RP-82, 118 p.

Halpern, C.B., Lutz, J.A., 2013. Canopy closure exerts weak controls on understory dynamics: a 30-year study of overstory–understory interactions. Ecol. Monogr. 83, 221–237.

Hanes, T.L., 1971. Succession after fire in the chaparral of southern California. Ecol. Monogr. 41, 27–52.

Harmon, M.E., 2001. Carbon sequestration in forests. J. For. 99, 24–29.

Harmon, M.E., Franklin, J.F., Swanson, F., Sollins, P., Gregory, S.V., Lamn, J.D., Anderson, N.H., Cline, S.P., Aumen, N.G., Sedell, J.K., Lienkaemper, G.W., Cromack Jr., K., Cummins, K.W., 1986. Ecology of coarse woody debris in temperate ecosystems. Adv. Ecol. Res. 15, 133–302.

Harmon, M.E., Sexton, J., 1996. Guidelines for Measurements of Woody Detritus in Forest Ecosystems. U.S. LTER Network Office, University of Washington, Seattle, 42 p (Publication No. 20).

Harmon, M.E., Bible, K., Ryan, M.G., Shaw, D.C., Chen, H., Klopatek, J.X., Li, X., 2004. Production, respiration, and overall carbon balance in an old-growth *Pseudotsuga-Tsuga* forest ecosystem. Ecosystems 7, 498–512.

Harr, R.D., 1982. Fog drip in the Bull Run municipal watershed, Oregon. Water Resour. Bull. 18, 785–789.

Henderson, J.A., Peter, D.H., Lesher, R.D., Shaw, D.C., 1989. Forested Plant Associations of the Olympic National Forest. USDA Forest Service R6-ECOL-TP 001-88, Portland, OR, 502 p.

Hikosaka, K., Hirose, T., 1997. Leaf angle as a strategy for light competition: Optimal and evolutionary stable light-extinction coefficient within a leaf canopy. Ecoscience 4, 501–507.

Horn, H., 1971. The Adaptive Geometry of Trees. Princeton University Press, Princeton, New Jersey, USA, 144 p.

Ishii, H., Ford, E.D., 2001. The role of epicormic shoot production in maintaining foliage in old *Pseudotsuga menziesii* (Douglas-fir) trees. Can. J. Bot. 79, 251–264.

Ishii, H., Tanabe, S., Hiura, T., 2004. Exploring the relationships among canopy structure, stand productivity and biodiversity of temperate forest ecosystems. Forest Science 50, 342–355.

Ishii, H., Asano, S., 2010. The role of crown architecture, leaf phenology and photosynthetic activity in promoting complementary use of light among coexisting species in temperate forests. Ecol. Res. 25, 715–722.

Ishii, H., Azuma, W., Nabeshima, E., 2013. The need for a canopy perspective to understand the importance of phenotypic plasticity for promoting species coexistence and light-use complementarity in forest ecosystems. Ecol. Res. 28, 191–198.

Jain, T.B., Graham, R.T., Adams, D., 2010. Carbon Concentrations and Carbon Pool Distributions in Dry, Moist, and Cold mid-aged Forests of the Rocky Mountains. USDA Forest Service RMRS-P-61, pp. 39–59.
Jameson, M.J., Robards, T.A., 2007. Coast redwood regeneration survival and growth in Mendocino County, California. Western J. Appl. For. 22, 171–175.
Kane, V.R., Gersonde, R.F., Lutz, J.A., McGaughey, R.J., Bakker, J.D., Franklin, J.F., 2011. Patch dynamics and the development of structural and spatial heterogeneity in Pacific Northwest forests. Can. J. For. Res. 41, 2276–2291.
Keeling, H.C., Phillips, O.L., 2007. The global relationship between forest productivity and biomass. Glob. Ecol. Biogeogr. 16, 618–631.
Keenan, R.J., Prescott, C.E., Kimmins, J.P., 1993. Mass and nutrient content of woody debris and forest floor in western red-cedar and western hemlock forests on northern Vancouver Island. Can. J. For. Res. 23, 1052–1059.
Keith, H., Mackey, B.G., Lindenmayer, D.B., 2009. Re-evaluation of forest biomass carbon stocks and lessons from the world's most carbon-dense forests. PNAS 106, 11635–11640.
Keith, H., Lindenmayer, D., Mackey, B., Blair, D., Carter, L., McBurney, L., Okada, S., Konishi-Nagano, T., 2014. Managing temperate forests for carbon storage: impacts of logging versus forest protection on carbon stocks. Ecosphere 5, 1–34.
Keller, E.A., MacDonald, A., Tally, T., Merrit, N.J., 1985. Effects of large debris on channel morphology and sediment storage in selected tributaries of Redwood Creek, northwestern California. In: Nolan, K.M., Kelsey, H.M., Maron, D.C. (Eds.), Geomorphic Processes and Aquatic Habitat in the Redwood Creek Basin, Northwestern California. U.S. Geological Survey Professional Paper 1454.
Kimmey, J.W., 1958. The Heart Rots of Redwood. USDA Forest Service, California Forest and Range Experimental Station, Forest Pest Leaflet 25, 7 p.
Kimmey, J.W., Hornibrook, E.M., 1952. Cull and Breakage Factors and Other Tree Measurement Tables for Redwood. USDA Forest Service, California Forest and Range Experimental Station, Forest Survey Release 13, 28 p.
Kimmey, J.W., Lightle, P.C., 1955. Fungi associated with cull in redwood. For. Sci. 1, 104–110.
King, D.A., 1994. Influence of light level on the growth and morphology of saplings in a Panamanian forest. Am. J. Bot. 81, 948–957.
Kira, T., Shidei, T., 1967. Primary production and turnover of organic matter in different forest ecosystems of the Western Pacific. Jpn. J. Ecol. 17, 70–87.
Koch, G.W., Sillett, S.C., Antoine, M.E., Williams, C.B., 2015. Growth maximization trumps maintenance of leaf conductance in the tallest angiosperm. Oecologia 177, 321–331.
Kojo, Y., 1987. A dendrochronological study of *Cryptomeria japonica* in Japan. Tree-Ring Bull. 47, 1–21.
Kuiper, L.C., 1988. The Structure of Natural Douglas-fir Forests in Western Washington and Western Oregon. Agricultural University Wageningen Papers 88, 5, 47 p.
Larjavaara, M., 2013. The world's tallest trees grow in thermally similar climates. New Phytol. 202, 344–349.
Larjavaara, M., Muller-Landau, H.C., 2011. Temperature explains global variation in biomass among humid old-growth forests. Glob. Ecol. Biogeogr. 21, 998–1006.
Larjavaara, M., Muller-Landau, H.C., 2013. Measuring tree height: a quantitative comparison of two common field methods in a moist tropical forest. Methods Ecol. Evol. 4, 793–801.
Lefsky, M.A., Cohen, W.B., Acker, S.A., Spies, T.A., Parker, G.G., Harding, D., 1999. LiDAR remote sensing of biophysical properties and canopy structure of forest of Douglas-fir and western hemlock. Remote Sens. Environ. 70, 339–361.
Leigh, E.G., Jr., Rand, A.S., Windsor, D.M. (Eds.), 1982. The Ecology of a Tropical Forest: Seasonal Rhythms and Long-Term Changes. Smithsonian Institution Press, Washington, DC, 468 p.
Leverenz, J.W., Hinckley, T.M., 1990. Shoot structure, leaf area index and productivity of evergreen conifer stands. Tree Physiol. 6, 135–149.
Long, J.N., Smith, F.W., 1992. Volume increment in *Pinus contorta* var. *latifolia*: the influence of stand development and crown dynamics. For. Ecol. Manage. 53, 53–64.
Lorimer, C.G., Porter, D.J., Madej, M.A., Stuart, J.D., Veirs Jr., S.D., Norman, S.P., O'Hara, K.L., Libby, W.J., 2009. Presettlement and modern disturbance regimes in coast redwood forests: implications for the conservation of old-growth stands. For. Ecol. Manage. 258, 1038–1054.
Luyssaert, S., Schulze, E., Borner, A., Knohl, A., Hessenmoller, D., Law, B.E., Ciais, P., Grace, J., 2008. Old-growth forests as global carbon sinks. Nature 455, 213–215.
Means, J.E., Hansen, H.A., Koerper, G.J., Alaback, P.B., Klopsch, M.W., 1994. Software for Computing Plant Biomass—Biopak Users Guide. USDA Forest Service PNW-GTR-340, 184 p.
Miller, E.E., Norman, J.M., 1971. A sunfleck theory for plant canopies II. Penumbra effect: intensity distributions along sunfleck segments. Agron. J. 63, 739–743.
Monsi, M., Saeki, T., 1953. Über den Lichtfaktor in den Pflanzengesellschaften und seine Bedeutung für die Stoffproduktion. Jpn. J. Bot. 14, 22–52 (Currently published as, Monsi, M., and T. Saeki. 2005. On the factor light in plant communities and its importance for matter production. Annals of Botany 95, 549–567).
Moore, P.T., Van Miegroet, H., Nicholas, N.S., 2007. Relative role of understory and overstory in carbon and nitrogen cycling in a southern Appalachian spruce-fir forest. Can. J. For. Res. 37, 2689–2700.
Moroni, M.T., Kelley, T.H., McLarin, M.L., 2010. Carbon in trees in Tasmanian State Forest. Int. J. For. Res. V. http://dx.doi.org/10.1155/2010/690462, 13 pages.
North, M.P., Hurteau, M.D., 2011. High-severity wildfire effects on carbon stocks and emissions in fuels treated and untreated forest. For. Ecol. Manage. 261, 1115–1120.
O'Brien, T.A., Sloan, L.C., Chuang, P.Y., Faloona, I.C., Johnstone, J.A., 2013. Multidecadal simulation of coastal fog with a regional climate model. Clim. Dyn. 40, 2801–2812.
O'Hara, K.L., Stancioiu, P.T., Spencer, M.A., 2007. Understory stump sprout development under variable canopy density and leaf area in coast redwood. For. Ecol. Manage. 244, 76–85.
Oldeman, R.A.A., 1983. Tropical rain forest, architecture, silvigenesis and diversity. In: Sutton, S.L. et al. (Eds.), Tropical Rain Forest: Ecology and Management. Blackwell, Oxford, p. 498.
Oldeman, R.A.A., 1990. Forests: Elements of Silvology. Springer-Verlag, Berlin, 624 p.
Oldham, A.R., Sillett, S.C., Tomescu, M.F., Koch, G.W., 2010. The hydrostatic gradient, not light availability drives height-related variation in *Sequoia Sempervirens* (*Cupressaceae*) leaf anatomy. Am. J. Bot. 97, 1087–1097.
Olivas, P.C., Oberbauer, S.F., Clark, D.B., Clark, D.A., Ryan, M.G., O'Brien, J.J., Ordonez, H., 2013. Comparison of direct and indirect methods for assessing leaf area index across a tropical rain forest landscape. Agric. For. Meteorol. 177, 110–116.
Pickett, S.T.A., Kempf, J.S., 1980. Branching patterns in forest shrubs and understory trees in relation to habitat. New Phytol. 86, 219–228.
Poorter, H., Niinemets, Ü., Poorter, L., Wright, I.J., Villar, R., 2009. Causes and consequences of variation in leaf mass per area (LMA): a meta-analysis. New Phytol. 182, 565–588.
PRISM Climate Group, 2012. Oregon State University. <http://prism.oregonstate.edu>.
Putz, F.E., Parker, G.G., Archibald, R.M., 1984. Mechanical abrasion and intercrown spacing. Am. Midl. Nat. 112, 24–28.
Ralph, F.M., Neiman, P.J., Wick, G.A., 2004. Satellite and CALJET aircraft observations of atmospheric rivers over the eastern North Pacific Ocean during the winter of 1997/98. Mon. Weather Rev. 132, 1721–1745.
Richards, P.W., 1952. The Tropical Rain Forest. Cambridge University Press, Cambridge, UK, 450 p.
Rosenzweig, M.L., 1968. Net primary productivity of terrestrial communities: prediction from climatological data. Am. Nat. 102, 67–74.
Rowntree, L., 2009. Forged by Fire: Lightning and Landscape at Big Sur. Bay Nature (Oct–Dec).
Roy, D.F., 1966. Silvical Characteristics of Redwood (*Sequoia Sempervirens* [D. Don] Endl.). USDA Forest Service PSW-RP-28, 20 p.
Ruth, R.H., 1954. Cascade Head Climatological Data 1936 to 1952. USDA Forest Service Pacific Northwest Research Station, Portland OR, 29 p.
Ryan, M.G., Binkley, D., Fownes, J.H., 1997. Age-related decline in forest productivity: pattern and process. Adv. Ecol. Res. 27, 213–262.
Sawyer, J.O., Sillett, S.C., Popenoe, J.H., LaBlanca, A., Sholars, T., Largent, D.L., Euphrat, F., Noss, R.F., Van Pelt, R., 2000. Characteristics of redwood forests. In: Noss, R.F. (Ed.), The Redwood Forest. Island Press, Covelo, CA (Chapter 3).
Sillett, S.C., Van Pelt, R., 2000. A redwood tree whose crown is a forest canopy. Northwest Sci. 74, 34–43.
Sillett, S.C., Van Pelt, R., 2007. Trunk reiteration promotes epiphytes and water storage in an old-growth redwood forest canopy. Ecol. Monogr. 77, 335–359.
Sillett, S.C., Van Pelt, R., Koch, G.W., Ambrose, A.R., Carroll, A.L., Antoine, M.E., Mifsud, B.M., 2010. Increasing wood production through old age in tall trees. For. Ecol. Manage. 259, 976–994.
Sillett, S.C., Van Pelt, R., Carroll, A.L., Kramer, R.D., Ambrose, A.R., Trask, D., 2015a. How do tree structure and old age affect growth potential of California redwoods? Ecol. Monogr. 85, 181–212.
Sillett, S.C., Van Pelt, R., Kramer, R.D., Carroll, A.L., Koch, G.W., 2015b. Biomass and growth potential of *Eucalyptus regnans* up to 100 m tall. For. Ecol. Manage. 348, 78–91.
Silverster, W.B., Orchard, T.A., 1999. The biology of kauri (*Agathis australis*) in New Zealand: Production, biomass, carbon storage, and litter fall in four forest remnants. NZ J. Bot. 37, 553–571.
Smith, W.B., Brand, G.L., 1983. Allometric Biomass Equations for 98 Species of Herbs Shrubs and Small Trees. USDA For. Serv. North Central Exp. Sta. Research Note NC-299, 8 p.
Smith, W.K., Knapp, A.K., Reiners, W.A., 1989. Penumbral effects on sunlight penetration in plant communities. Ecology 70, 1603–1609.
Smith, W.K., Brewer, C.A., 1994. The adaptive importance of shoot and crown architecture in conifer trees. Am. Nat. 143, 528–532.
Smithwick, E.A., Harmon, M.E., Remillard, S.M., Acker, S.A., Franklin, J.F., 2002. Potential upper bounds of carbon stores in forests of the Pacific Northwest. Ecol. Appl. 12, 1303–1317.
Sohn, J., McElhinny, C., Grove, S., Hilbig, E., Bauhus, J., 2013. A simplified inventory approach for estimating carbon in coarse woody debris in high-biomass forests. Pap. Proc. R. Soc. Tas. 147, 15–23.
Sollins, P., Cline, S.P., Verhoeven, T., Sachs, D., Spycher, G., 1987. Patterns of log decay in old-growth Douglas-fir forests. Can. J. For. Res. 17, 1585–1595.
Spies, T.A., Franklin, J.F., Thomas, T.B., 1988. Coarse woody debris in Douglas-fir forests of western Oregon and Washington. Ecology 69, 1689–1702.
Spies, T.A., Franklin, J.F., Klopsch, M., 1990. Canopy gaps in Douglas-fir forests of the Cascade Mountains. Can. J. For. Res. 20, 649–658.
Spies, T.A., Pabst, R.J., Gray, A.N., 1999. Shrub and herb community responses to experimental canopy gaps in Douglas-fir forests (Abstract). In: The Ecological Society of America 84th Annual Meeting: Legacies, Landscapes and Limits: Bridging Borders; 1999 August 8–12; Spokane, WA. Ecological Society of America, Washington, DC, p. 309.
Stephens, S.L., Fry, D.L., 2005. Fire history in coast redwood stands in the northeastern Santa Cruz Mountains, California. Fire Ecol. 1, 2–19.
Tng, D.Y.P., Williamson, G.J., Jordan, G.J., Bowman, D.M.J.S., 2012. Giant eucalypts – globally unique fire-adapted rain forest trees? New Phytol. 196, 1001–1014.

Tng, D.Y.P., Goosem, S., Jordan, G.J., Bowman, D.M.J.S., 2014. Letting giants be – rethinking active fire management of old-growth eucalypt forest in the Australian tropics. J. Appl. Ecol. 51, 555–559.
Triska, E.J., Cromack Jr., K., 1980. The roles of wood debris in forests and streams. In: Waring, R.H. (Ed.), Forests: Fresh Perspectives from Ecosystem Analysis. Proceedings 40th Biology Colloquium (1979). Oregon State University Press, Corvallis, OR, pp. 171–190.
Turner, J., Long, J.N., 1975. Accumulation of organic matter in a series of Douglas-fir stands. Can. J. For. Res. 5, 681–690.
USGS, 2015. The Pacific Coastal Fog Project: Developing Ecologically Relevant Fog Datasets. Western Geographic Science Center. United States Geological Survey. <http://geography.wr.usgs.gov/science/eco.html>.
Van Pelt, R., 2001. Forest Giants of the Pacific Coast. University of Washington Press, Seattle, Washington, USA, 200 p.
Van Pelt, R., 2007. Identifying Mature and Old Forests in Western Washington. Washington State Department of Natural Resources, Olympia WA, USA, 106 p.
Van Pelt, R., North, M.P., 1999. Testing a ground-based canopy model using the Wind River Canopy Crane. Selbyana 20, 357–362.
Van Pelt, R., Franklin, J.F., 2000. Influence of canopy structure on the understory environment in tall, old-growth, conifer forests. Can. J. For. Res. 30, 1231–1245.
Van Pelt, R., Nadkarni, N.M., 2004. Development of canopy structure in *Pseudotsuga menziesii* forests in the southern Washington Cascades. For. Sci. 50, 326–341.
Van Pelt, R., Sillett, S.C., Nadkarni, N.M., 2004. Quantifying and visualizing canopy structure in tall forests: methods and a case study. In: Lowman, M., Rinker, B. (Eds.), Forest Canopies, second ed. Elsevier, Boston, MA, pp. 49–72.
Van Pelt, R., Sillett, S.C., 2008. Crown development of coastal *Pseudosuga menziesii*, including a conceptual model for tall conifers. Ecol. Monogr. 78, 283–311.
Veblen, T.T., Ashton, D.H., 1982. The regeneration status of *Fitzroya cupressoides* in the Cordillera Pelada, Chile. Biol. Conserv. 23, 141–161.
Veirs, S.D., 1982. Coast redwood forest: stand dynamics, successional status, and the role of fire. In: Means, J.E. (Ed.), Proceedings of the Symposium on Forest Succession and Stand Development in the Pacific Northwest. Oregon State University, Corvallis, OR, USA, pp. 119–141.
Waring, R.H., 1983. Estimating forest growth and efficiency in relation to canopy leaf area. Adv. Ecol. Res. 13, 327–354.
Waring, R.H., Franklin, J.F., 1979. Evergreen coniferous forests of the Pacific Northwest. Science 204, 1380–1386.
Westman, W.E., Whittaker, R.H., 1975. The pygmy forest region of northern California: studies on biomass and primary productivity. J. Ecol. 63, 493–520.
Whittaker, R.H., 1970. Communities and Ecosystems. Macmillan, New York, 162 p.
Wood, S.W., Hua, Q., Allen, K.J., Bowman, D.M.J.S., 2010. Age and growth of a fire prone Tasmanian temperate old-growth forest stand dominated by *Eucalyptus regnans*, the world's tallest angiosperm. For. Ecol. Manage. 260, 438–447.
Xu, C.-Y., Turnbull, M.H., Tissue, D.T., Lewis, J.D., Carson, R., Schuster, W.S.F., Whitehead, D., Walcroft, A.S., Li, J., Griffin, K.L., 2012. Age-related decline of stand biomass accumulation is primarily due to mortality and not to reduction in NPP associated with individual tree physiology, tree growth or stand structure in a *Quercus*-dominated forest. J. Ecol. 100, 428–440.
Zhang, J., Powers, R.F., Skinner, C.N., 2010. To manage or not to manage the role of silviculture in sequestering carbon in the specter of climate change. In: Jain, T. B., Graham, R.T., Sandquist, J. (Eds.), Integrated Management of Carbon Sequestration and Biomass Utilization Opportunities in a Changing Climate: Proceedings of the 2009 National Silviculture Workshop, 2009 June 15–18, Boise, ID. USDA Forest Service RMRS-P-61, p. 2929.
Zhu, Y., Newell, R., 1998. A proposed algorithm for moisture fluxes from atmospheric rivers. Mon. Weather Rev. 126, 725–735.